

## NCWF-2 Probabilistic Nowcasts

Dan Megenhardt<sup>1</sup>, C. Mueller, S. Trier, D. Ahijevych, and N. Rehak  
National Center for Atmospheric Research

### 1. Introduction

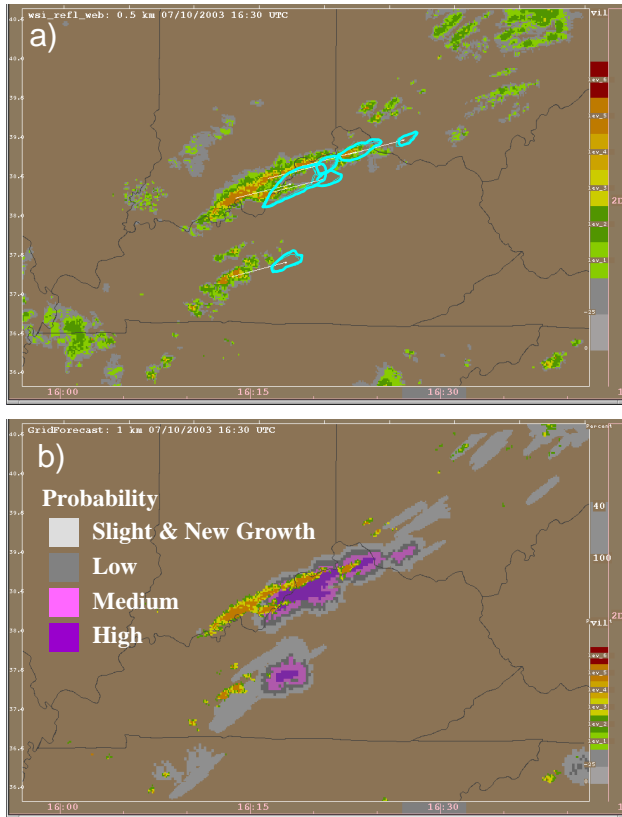


Figure 1. Examples of 1-hr forecast from NCWF-1 and NCWF-2. (a) shows NCWF-1 forecast presentation, National Convective Weather Detection (NCWD) is the background field and the cyan polygons indicate the one hour forecast position. (b) shows a preliminary presentation of NCWF-2 forecast probabilities (background gray and purple shades) and current NCWD (level 3 or greater).

This paper describes the National Convective Weather Forecast version 2 (NCWF-2), an evolving software system that provides probabilistic one and two hour nowcasts of convective storm location and intensity. NCWF-2 combines meteorological observations, feature detection algorithms, and Rapid Update Cycle (RUC) numerical weather prediction output to provide routine nowcasts of thunderstorm position. NCWF-2 is developed by the National Center for Atmospheric Research with prime funding from the Federal Aviation Administration<sup>2</sup> and as part of the Aviation Weather Research Program's Convective Weather Product Development team that includes collaboration with MIT Lincoln Laboratory, NOAA National Severe Storms Laboratory, and NOAA National Weather Service Aviation Weather Center (AWC).

The current operational version of NCWF (Megenhardt et. al., 2000) shows the convective hazard detection field (called National Convective Weather Detection - NCWD) and a binary forecast of storm location with a one hour lead time (NCWF-1, see Fig. 1). This operational product was first available to users in 1998 as an experimental product and became operational in 2000. Problems associated with this product include: long lead-times before the first extrapolations are provided, extrapolation vectors turning on and off if storms are near the threshold size limit, no extrapolation on small storms that do not meet size thresholds, and sporadic motion vectors especially in the southern regions of the country where steering flow winds are weak. Many of the problems associated with NCWF-1 motion vectors are directly addressed in NCWF-2 by improved quality control and use of the RUC steering level winds. In addition to problems with the motion vectors, the NCWF-1

<sup>1</sup> Corresponding author address: Dan Megenhardt, NCAR, P.O. Box 3000 Boulder, CO 80307; email: [hardt@ucar.edu](mailto:hardt@ucar.edu)

<sup>2</sup> FAA support is presently through the Aviation Weather Research Program (AWRP) as part of the Convective Weather Product Development Team (Wolfson et. al. 1997). Additional support has been received from the Army Test and Evaluation Command (ATEC) and National Science Foundation.

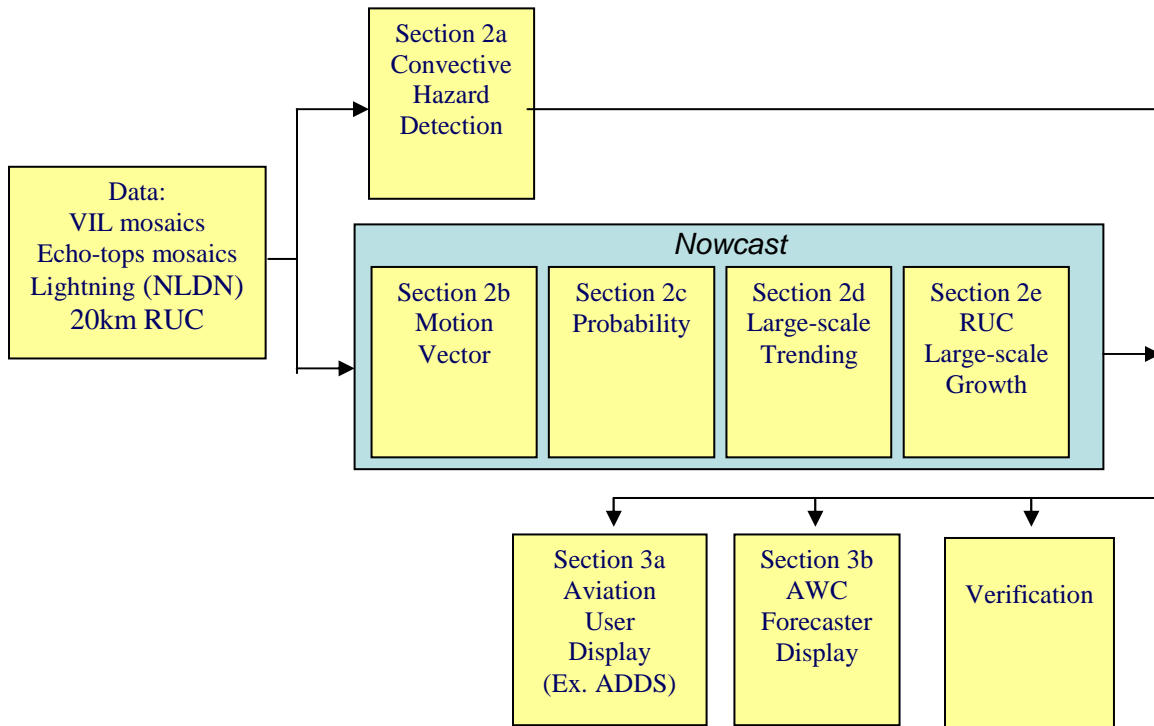


Figure 2. Schematic for NCWF-2 processing. Details of the processing are found in the text under the indicated Section.

nowcasts are limited because of uncertainty in the polygon shapes and inability to forecast initiation or forecast regions of change (growth and decay). The deterministic forecast is useful for tactical decision making (steering flights around storms). However, depending on the organization of convection, forecast skill rapidly decreases after the first hour. Probabilities allow quantification of uncertainty inherent in the forecasts.

The atmospheric science community generally agrees that probabilities are the most meaningful method for forecasting convection because they provide a method to quantify uncertainty. In addition, probabilities provide a methodology (or common unit) to combine observational-based forecasts with NWP and forecaster input. The National Research Council's report on Weather Forecasting Accuracy for FAA Traffic Flow Management states that, "Because accurate deterministic 2- to 6-hour forecasts are not available, it is necessary to develop probabilistic forecasts that can readily be used by both humans and automated air traffic management decision support tools." One of the critical tasks was defined as: "Defining probabilistic forecasting and determining how it could best be applied in air traffic management." Currently, probability forecasts from the perspectives of the forecaster, aviation user, or verification analyst are not well understood. In order to move forward,

experimental probabilistic forecasts should be made available to the user community and verification groups in order to determine strengths and weaknesses. The NCWF-2 is seen as a preliminary step towards a continuous 0-6 hr probabilistic forecast. Thus, the NCWF-2 provides probabilistic nowcasts at 1 and 2 hrs for the aviation community and 1 to 4 hr forecasts as an aid to forecasters producing the AWC's Convective SIGMET and Collaborative Convection Forecast Products (CCFP – Hudson and Foss, 2002).

Section 2 of this paper describes and illustrates NCWF-2 methodology. Section 3 shows draft presentations for display on Aviation Digital Data Service (ADDS – Sherretz et al. 2002) and AWC Forecaster workstations, and Section 4 provides a brief discussion.

## 2. NCWF-2 Methodology

The steps in producing the nowcasts are briefly reviewed here to give an overview of the entire system. Figure 2 provides a generalized schematic of the NCWF-2 system. Operational data sets used in the system include national mosaics of WSR-88D level 3 radar fields (Klazura and Imy, 1993), national lightning detection network (NLDN), and Rapid Update Cycle (RUC) numerical model fields output. These data are

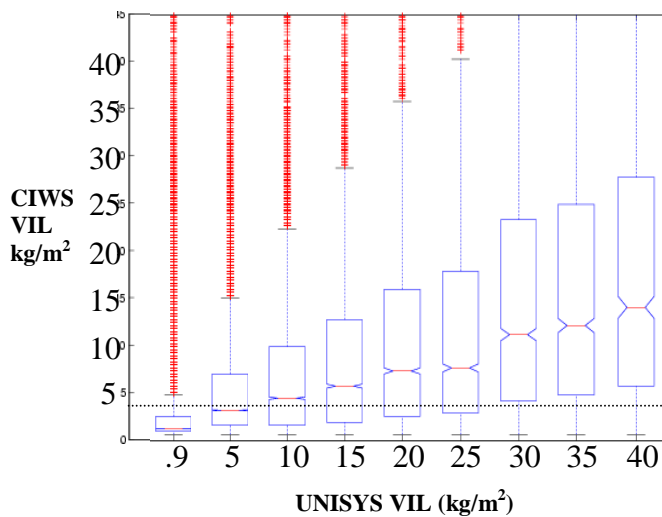


Figure 3. Box plots comparing UNISYS VIL with CIWS VIL for June, 26, 2002 (24 hrs of data) are shown. See text for details.

used for convective hazard detection and nowcast generations. The steps in the nowcast generation are: calculation of motion vectors based on RUC winds and storm tracking, calculation of probabilities based on spatial distribution of radar return, modification of probabilities based on trends in large-scale dissipation, and addition of low probabilities for convection in regions where storm development is favorable. Verification is done both internally and by NOAA Forecast System Laboratory (FSL) Real-time Verification System (RTVS – Mahoney et al. 2002). Finally, the data are sent to experimental ADDS or to the AWC forecaster's workstation.

#### a) Hazard Detection

The diagnostic analysis combines WSR-88D national radar mosaics (provided by NOAA with mosaics created and distributed by UNISYS) and cloud-to-ground lightning (provided by Global Atmospheric Inc). The Convective Hazard Detection field (shown in Fig. 1a) is depicted based on a standard 6 level VIP categories.

The Vertically Integrated Liquid (VIL) data are provided in the WSR-88D Level 3 product stream and are mapped to a national mosaic by UNISYS. The VIL field uses an empirical formula to derive liquid water content from radar reflectivity at each elevation. The data are then integrated with height to obtain VIL. VIL is generally accepted by the aviation community as

a good convection diagnostic (Evans and Ducot, 1994, Crowe and Miller, 1999, Robinson et al., 2002). Because VIL is an integrated product, it provides a proxy to vertical storm development and minimizes the effects of bright-band echo, Anomalous Propagation (AP) and ground clutter. The WSR-88D level 3 product stream provides VIL data with a horizontal resolution of 4 km (Kluzura and Imy, 1993). The VIL data available at the AWC are divided by the NWS into 5 kg-m<sup>-2</sup> intervals. The first interval is 0.9 to 5 kg-m<sup>-2</sup>, the following bins are provided at 5 kg-m<sup>-2</sup> intervals and labeled with the minimum value. Troxel and Engholm (1990) suggested conversion of VIL into interest images representing the standard VIP levels using the values in Table 1 (Hallowell et al. 1999). The values that are used by the NCWF-2 are indicated. The bins provided by NWS are not ideal. There is not enough information in the NWS-VIL data stream to differentiate VIP level 1 and level 2 returns. In addition, the mapping requires that the NCWD VIP 3 returns are based on a threshold of 5 kg-m<sup>-2</sup> instead of 3.5 kg-m<sup>-2</sup> suggested by research. In order to better quantify the NWS-VIL data set, a comparison was done using the MIT/LL high resolution VIL (Robinson et al. 2002) over the Corridor Integrated Weather System (CIWS – Evans et al. 2002) domain. A 24hr period that contained a good deal of convection over the NE corridor was used. The MIT/LL VIL data are calculated based on the WSR-88D level-2 radial data. The data are quality controlled and aligned in time prior to the vertical integration. The final mosaics have a resolution of 1 km and are updated every 2.5 min. Figure 3 shows standard box plots of CIWS-VIL for each NWS-VIL interval. In the box plots, the middle line (red) is the median (or the 0.50th quantile); the lines at the bottom and top of the boxes are the 0.25<sup>th</sup> and 0.90<sup>th</sup> quantile values, the small lines at the top represent the extremes and the red crosses are outliers. The variability shown in the box plots is largely due to the difference in resolution between the data sets and is expected. The UNISYS-VIL 5kg-m<sup>-2</sup> bin has an average CIWS-VIL value of ~3 kg-m<sup>-2</sup>. This comparison suggests that the 5 kg-m<sup>-2</sup> UNISYS-VIL value that is used in NCWF compares favorably with a 3.5 kg m<sup>-2</sup> CIWS-VIL value. These plots and review of data from many cases indicate that the UNISYS-VIL values are much higher than those indicated by the CIWS-VIL and that the UNISYS-VIL 5 kg m<sup>-2</sup> tends to overestimate the area of VIP3 as compared to CIWS-VIL.

Some example UNISYS-VIL and Echo-tops fields are shown in Figs. 4a and 4b respectively. VIL data are removed in regions with radar echo tops less than or equal to 15,000 ft. The majority of data removed at the 15,000 ft agl level are light precipitation that is not associated with summer-

| NWS "VIP" level (ASR reflectivity) | VIL (Kg m <sup>-2</sup> ) | Nexrad Level-3 VIL (Kg m <sup>-2</sup> ) | Lightning Rate (per 10 min) |
|------------------------------------|---------------------------|--|-----------------------------|
| 1 (18 dBZ)                         | 0.14                      | 0.9                                      | -                           |
| 2 (30 dBZ)                         | 0.76                      |  |                             |
| 3 (41 dBZ)                         | 3.5                       | 5  | 3-5                         |
| 4 (46 dBZ)                         | 6.9                       | 10                                       | 6-14                        |
| 5 (50 dBZ)                         | 12.0                      | 15                                       | 15 – 20                     |
| 6 (57 dBZ)                         | 32.                       | 30                                       | > 20                        |

Table 1. The first two columns show conversion values between VIP and VIL levels from Hallowell et al. (1999). The last 2 column shows the NCWF-2 conversion values between VIL, lightning rate and VIP.

time convection. In addition, this procedure removes most AP and ground clutter echoes. An additional field is calculated at an elevation threshold of 30,000 ft agl. This field is for display

only and is for commercial airline traffic that can often fly over dissipating low-level storms.

Cloud to ground lightning from the National Lightning Detection Network (NLDN – Cummins et al. 1998) provides a timely indication of convection. The NLDN network uses 105 lightning sensors that detect electro-magnetic signals produced by cloud to ground lightning discharges. This information is transmitted via satellite to a central processor and then distributed by Global Atmospheric Inc. within seconds. Individual radar data within the national mosaics are often late or missing. The mosaic itself is as much as 15-25 min old by the time it is distributed to outside users. The cloud-to-ground lightning data are updated continuously and provide an indication of updraft locations. This constant update allows frequent updates with current data. Weber et al. (1998) found a moderate correlation between the NLDN lightning and the radar VIL field. NCWF-2 maps the lightning data to a 4 km grid by summing the number of strikes that occurred in the past 10 minutes within 8 km of each point (see Fig. 4c). The radius of influences, time, and rate values (shown in Table 1) were all determined by visual and statistical comparisons of lightning rate fields and UNISYS-VIL data. The VIL and lightning

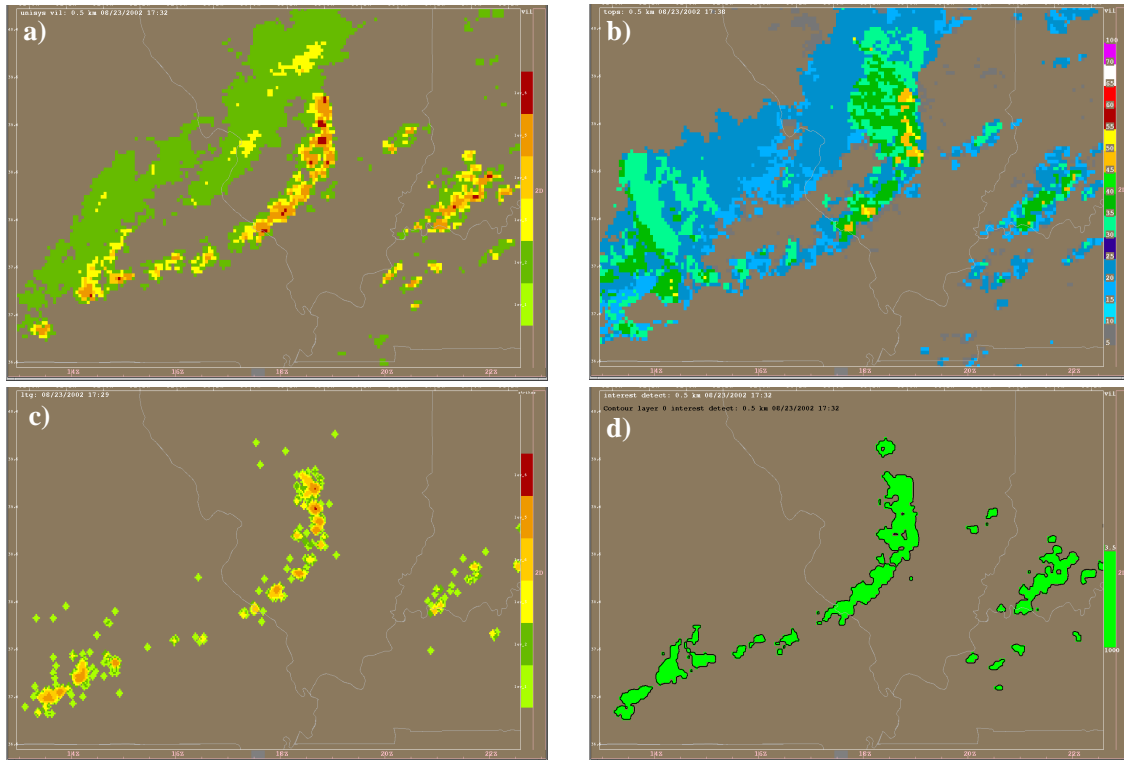


Figure 4. Example radar and lightning data sets; (a) shows 4km UNISYS- VIL, (b) shows 4 km echo tops, (c) lightning rate, and (d) the binary NCWD that is used for validation.

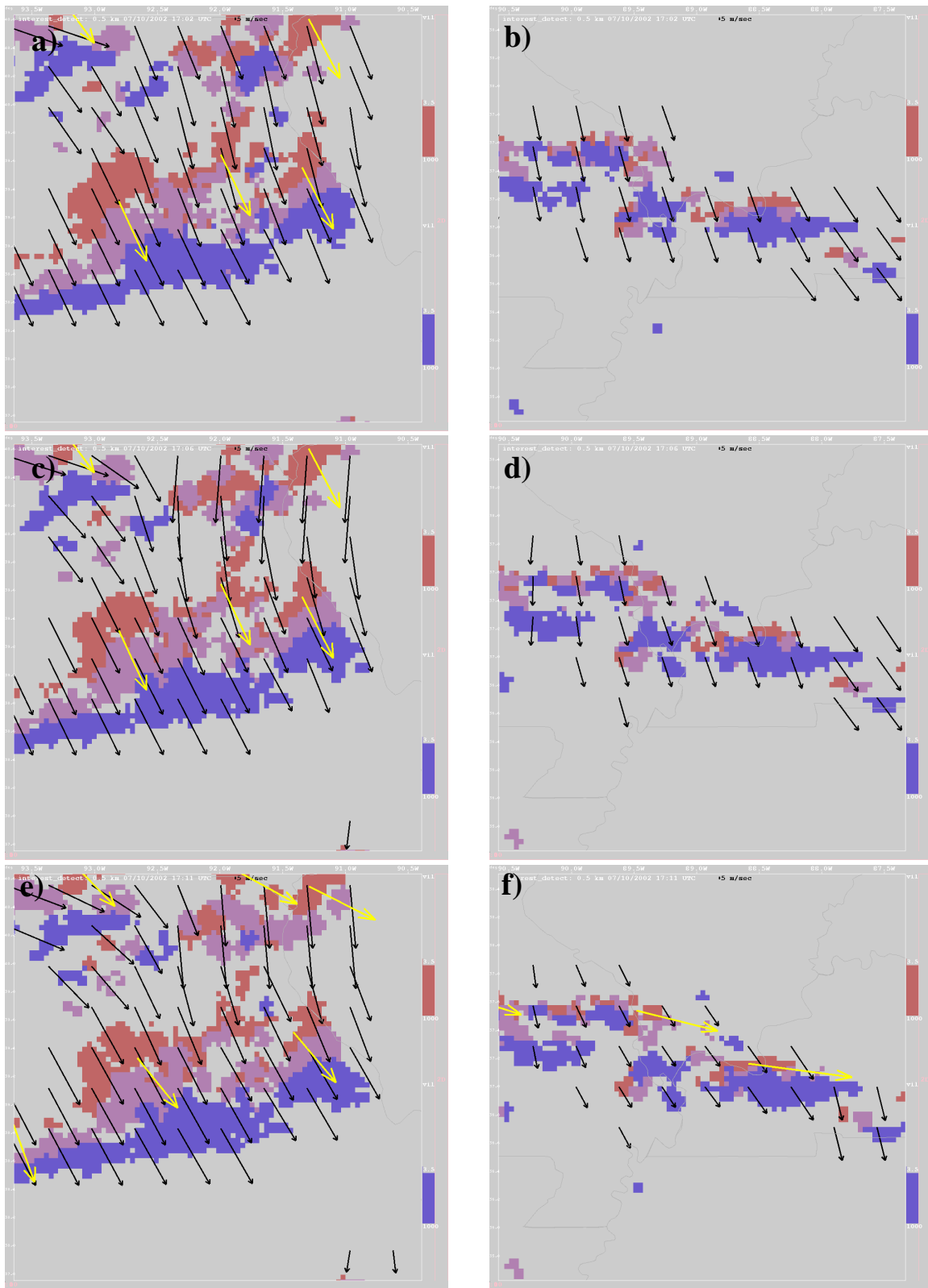


Figure 5. The binary NCWD is plotted at 30 min intervals. The red NCWD corresponds to the motion vectors. The purple NCWD is 30 min later and the blue NCWD an hour later. The black motion vectors correspond to the NCWF-2 and the yellow NCWF-1.

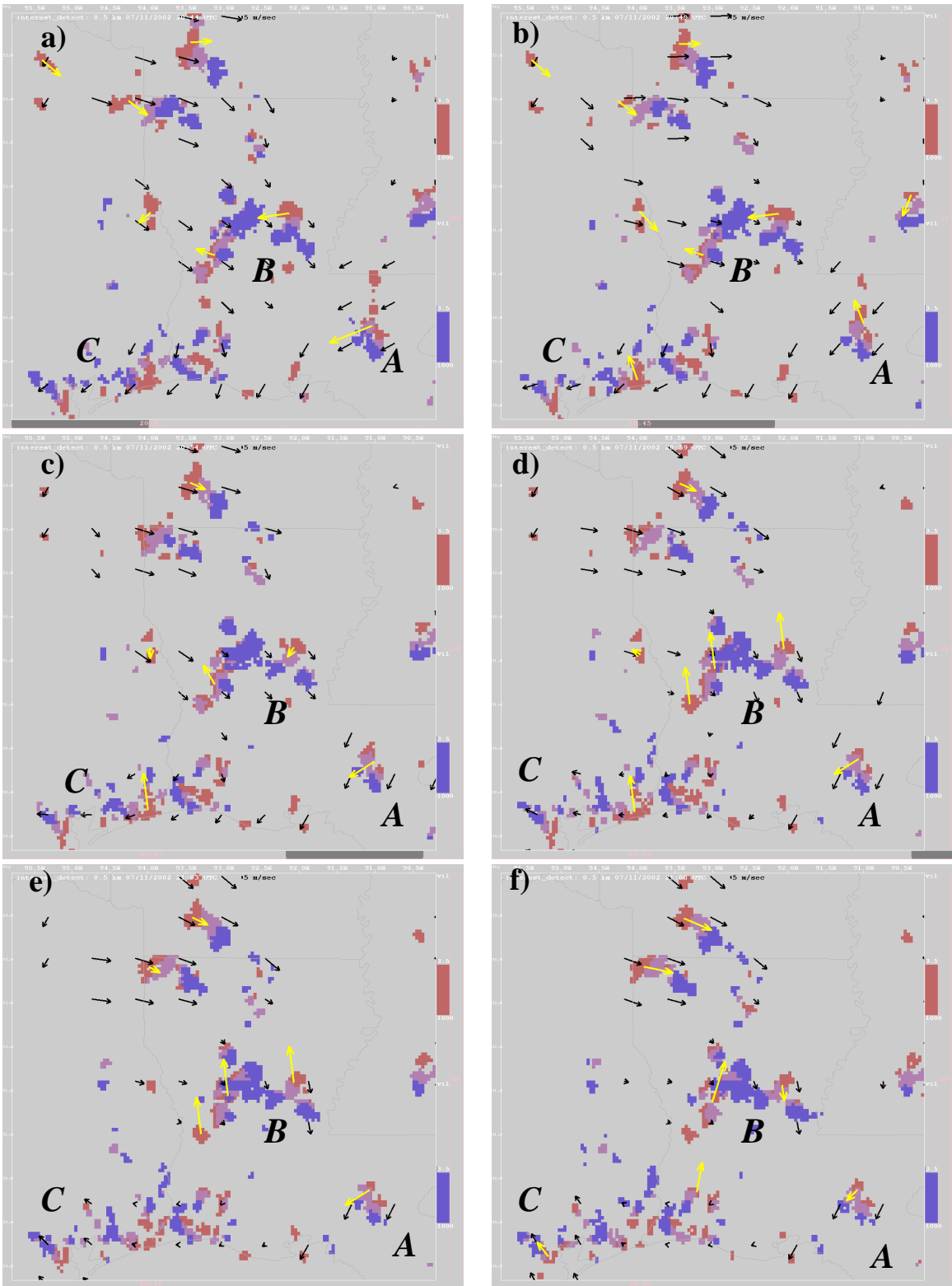


Figure 6. Same as Figure 5 except data are shown at 5 min intervals centered on Louisiana.

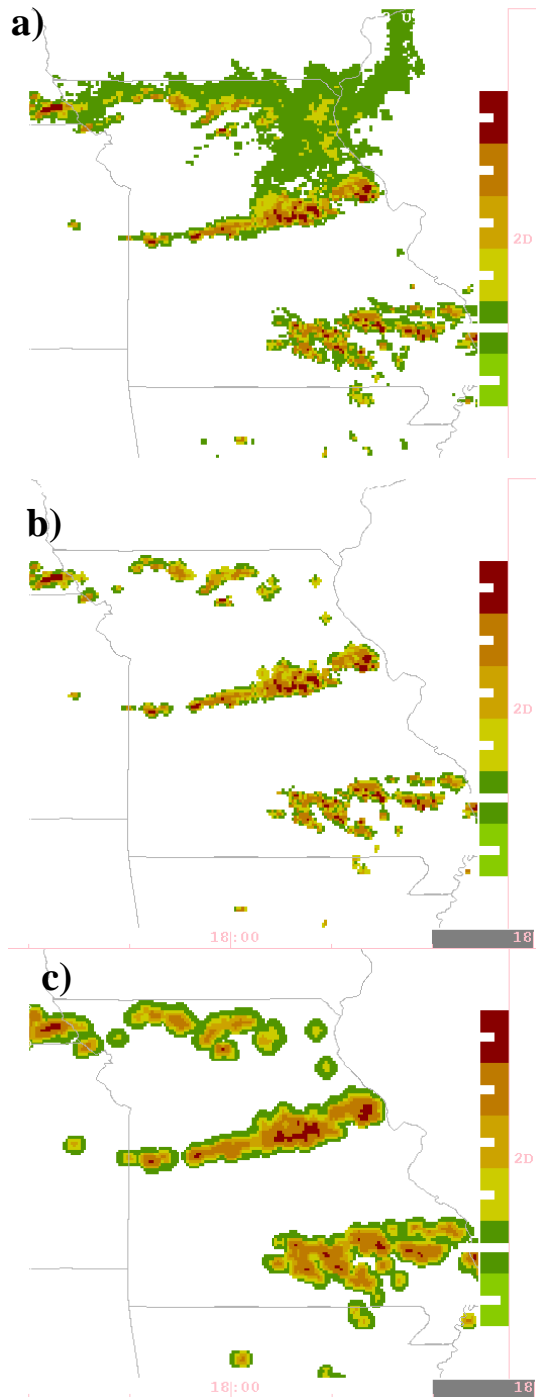


Figure 7. The processing steps for filtering the NCWD prior to tracking are shown. (a) is the NCWD field that is displayed on ADDS. (b) shows the NCWD field after the stratiform echo is removed. (c) shows the field prior to extrapolation after the elliptical filter is run.

data are mapped to the hazard detection field using the values shown in Table 1. If there is a discrepancy between the convective hazard detection level indicated by the lightning data or the VIL, data from the maximum level are used. Thus, a VIP level 3 (which is considered the threshold for a convective hazard) is associated with a VIL of greater or equal to  $5 \text{ kg}\cdot\text{m}^{-2}$  or lightning rate greater than or equal to 3 strokes over 10 minutes. The lightning is added in the same manner for both the 15,000 ft and 30,000 ft agl NCWD fields. Typically, the lightning data addition to the NCWD is along the leading edge of storms and in regions where radars are missing. The binary-NCWD field (Fig 4d) is used as the observed field for validation of the NCWF-2, Convective SIGMETS, and CCFP forecasts. The binary-NCWD is set to “yes” for convection (green area in Fig 4d) if the VIP value is 3 or greater (see Table 1) and if the region is considered convective based on a convective-stratiform partitioner (Steiner et al. 1985). Information about the convective-stratiform partitioner is found in the next section.

#### b) Motion Vectors

Much work has gone into improving the motion vectors used in the NCWF-1 in development of the NCWF-2 system. Comparisons between motion vectors used in NCWF-1 and NCWF-2 are shown in Figs. 5 and 6. The yellow vectors indicate NCWF-1 motions and the black vectors indicate the motions used for NCWF-2. The vectors in Figs. 5 and 6 are scaled such that their length represents the distance a storm is extrapolated during a 60 min period. The background shows binary-NCWD for the forecast time in red, NCWD at 30 min after the forecast time in blue, and 60 min after in purple. This display allows quick assessment of the quality of the motions; a perfect extrapolation should show a vector that extends from the red to the purple regions.

Figures 5a, c and e show examples of good motion vectors from both NCWF-1 and NCWF-2. The motion vectors from both systems are in agreement (especially for the southern storm area). The data are shown at 5 min intervals and the motions remain steady between the three periods. The NCWF-1 vectors are tied to individual storm centers. The NCWF-2 vectors are mapped to a 4 km grid. Mapping the motion vectors to a regular grid allows a field of data to be extrapolated (as in NCWF-2) instead of an individual storm (as in NCWF-1). It also allows a smooth transition between motion vectors. The motion vectors in the northern region of Figs. 5a, c, and e show one of the tracking problems that occurred frequently in NCWF-1. During this 10 min period, NCWF-1 shows that the motion

vectors for this northerly storm change by about 60°. This is due to errors in tracking. The NCWF-2 shows much less change over the 10 min period and correctly assigns a southern motion to the storms.

Figures 5b, d, and f are at the same times as 5a, c, and e, respectively, but in a different location where a line of storms is developing. One of the biggest criticisms of NCWF-1 was the length of time required before a motion vector was assigned. This is not a problem with NCWF-2 because as soon as a storm forms, it is assigned motion vectors based on the RUC steering flow wind (RUC pressure level of 750 mb, which translates to altitude of ~3 km agl). This steering-flow altitude level is consistent with values found by Wilson and Megenhardt (1997) in Florida for small storms. Figures 5b and d show regions where NCWF-1 motion vectors are not available, but the NCWF-2 motion vectors based on RUC are quite good. Figure 5f shows another problem that often occurred with NCWF-1, the first motion vectors are clearly incorrect. The more stringent quality controls on NCWF-2 motion vectors help eliminate this problem. Although RUC winds are good for initial storms, they are not appropriate as storms begin to propagate. When a "good" TITAN vector becomes available, it will be used in place of the RUC winds.

A difficult situation for tracking algorithms is the slow moving weakly forced convection that is prevalent throughout the summer in the southeastern part of the United States. Figure 6 shows a series of data at 5 min intervals over Louisiana. The NCWF-1 vectors are inconsistent in time (region A), often incorrect (region B), and blink in and out (region C). The NCWF-2 vectors show a great deal of improvement because the motions are consistent and generally accurate.

The following sub-sections - Data Filters, Thunderstorm Identification and Tracking, and Integration of TITAN and RUC Motions - document the steps used in NCWF-2 to determine the motion vector field.

#### 1) DATA FILTERS

NCWD data are filtered to remove stratiform echo and perishable scales. Figure 7 shows the results of applying the stratiform-convective

partitioner (Steiner et al. 1985) to the VIL field (Fig. 7a and b). Stratiform regions are removed based on texture and intensity. The algorithm detects peaks in VIL generally associated with convection. Removal of stratiform return allows the software to capture the motion of the convective elements that generally move with a different motion than stratiform regions. The stratiform return is not removed from the final displayed detection field, it is only removed from the field used to calculate the motion vectors and to provide an observation for verification.

Perishable scales are removed from the data by using an elliptical filter. Battan (1959) first reported that the movement of individual storm cells in a squall line is to the left of the squall line's motion or propagation and that the individual storm elements were short lived (tens of minutes) in comparison to the squall line itself that might have a lifetime of several hours. Wilson (1966) showed that the lifetime and echo motion was dependant on the scale of the convective element. Bellon and Zawadzki (1994) proposed using spatial averaging with a length scale that increased in size based on forecast lead time to filter out small, perishable scales. Wolfson et al. (1998) suggested the use of an elliptical filter to remove perishable scales. The elliptical filter maintains the linear structure of storm systems which allows tracking algorithms to capture the propagation instead of the individual cell motions. Figure 7c is the result of applying the elliptical filter used by NCWF-2 to the stratiform-filtered field (Fig 7b). This filtered NCWD field is only used for determining motion vectors.

#### 2) THUNDERSTORM IDENTIFICATION AND TRACKING

The Thunderstorm Identification Tracking and Nowcasting algorithm (TITAN, Dixon and Wiener 1993) determines motion vectors of storms. TITAN tracks individual storms when processing high-resolution (1km) unfiltered radar data or storm complexes (as is the case of NCWF-2) when the input data are in a lower resolution (4km) and filtered. The algorithm components that are used in NCWF-2 are storm identification, tracking, and calculation of motion vectors.

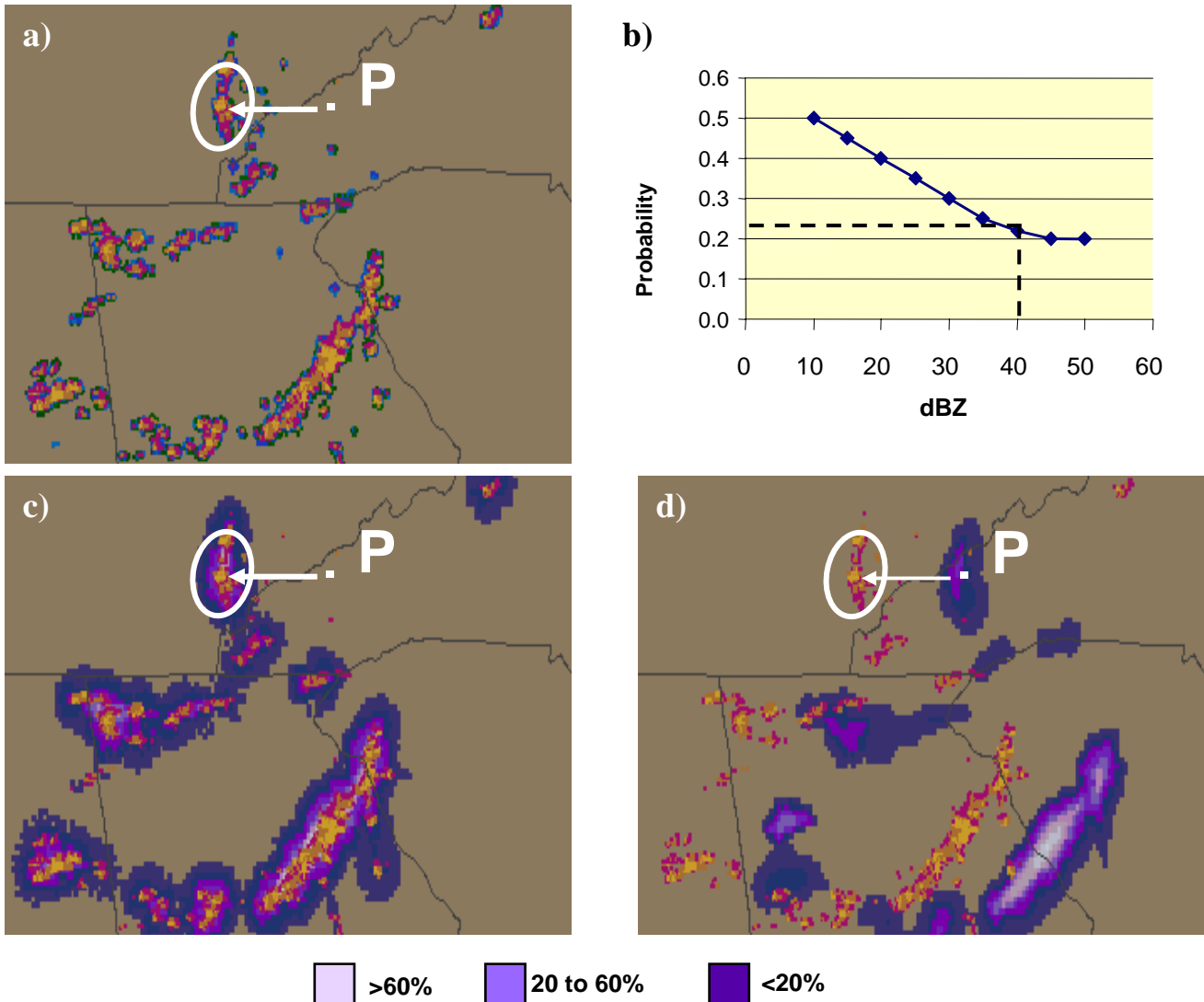


Figure 8. (a) and (b) illustrate the processing steps for determining probability based on GZ's Local Lagrangian technique. (c) and (d) show the NCWF-2 probabilities. The yellow/brown colors in (a), (c), and (d) indicate reflectivities. The probability distribution shown in (b) is for a point P [shown in (a), (c), and (d)]. The arrow in (a), (c), and (d) indicates the trajectory based on storm motion that is used to determine the probability distribution function (PDF) at point P. The PDF (spatial distribution) of storms is determined for point P within a region encompassed by the white circle shown in (a), (c), and (d). (c) and (d) indicate a field of probabilities in shades of purple that are determined for a single threshold level [shown as the dashed line in (b)]. The probability field is calculated based on conditions at forecast time (c) and extrapolated based on the NCWF-2 motion vectors.

The storm identification component is applied to the 2-dimensional elliptical-filtered NCWD field. In the case of NCWF-2, storm areas are required to be at least 500 km<sup>2</sup>. This size limitation was problematic with NCWF-1 because forecasts were only provided if storms met the size requirement and were tracked long enough to provide a good forecast vector (often 30 minutes or more). This is not the case for NCWF-2 because TITAN vectors are used in conjunction

with RUC winds; therefore, forecasts are not tied to TITAN storm detections as in NCWF-1. Several sensitivity studies were conducted while developing NCWF-2 to determine if the storm area requirement could be decreased. The results of decreasing the size limit consistently provided poorer results. Each 4 km grid has an area of 16 km<sup>2</sup> thus a 500 km<sup>2</sup> storm is effectively 30 consecutive grid points. When the algorithm was set to track cells with areas smaller than 500

km<sup>2</sup>, motions due to growth or mismatch in the tracking often produced vectors that were not as accurate as the RUC steering flow winds. As a result, the RUC steering flow is used for small storms and TITAN is used for the larger storm complexes. Often in the case of long-lived linear storms, the propagation motion along the line of storms varies. TITAN automatically splits storm complexes based on user-defined thresholds, thus preventing large linear systems from being extrapolated based on one motion vector.

Tracking of the storms over time is a two step process. The first step checks to determine the overlap between storms identified at two consecutive periods (in NCWF-2 a 10 min time interval is used). If the overlap is 30% or more, the storms are considered connected. If an overlap does not exist, a cost function is run that minimizes the change in volume and the distance between the storm centroids. TITAN handles storm splits and mergers, so that the storm history is preserved. Storm tracks are limited by a user set maximum speed value.

Once there is a logical connection calculated between the storms, storm motions are determined. In the case of an individual storm that has not split or merged, the storm motion is determined based on a time-weighted function of distance traveled over the interval between data fields. For NCWF-2, 20 min of history (a storm identified and tracked over 2 consecutive time periods) are required for a motion vector to be calculated. When available, 120 min of history are included in the motion calculation. In order to minimize the effects of false-motions, the distance a storm travels when there is a split or merger is adjusted. The translation or adjustment is done between the past storm track and the centroid of the new merged or split storm. One can think of the translation as a realignment of the storm track to minimize cross track motion. Finally, several quality checks are completed before a vector is considered valid. One of the most effective checks is to compare the distance a storm moves during the most recent time interval with the median distance traveled based on history. If the distance traveled is more than twice the median distance (or the storm motion increases by a factor of two), the new distance is set to the median value.

### 3) Integration of TITAN and RUC Motions

NCWF-2 produces an echo-extrapolation vector field in the vicinity of storms based on the RUC winds and TITAN echo extrapolation vectors. The vector field is based on a two step process. In the first step, the RUC and TITAN vectors are used to populate the grid. The second step

ensures that the vectors do not change radically during an individual time period.

In the first step, the RUC 750 mb wind, which in the summer translates to an altitude of ~3 km agl, is used as the steering flow (although this method provides good motion vectors in the summer, evaluation needs to be done for spring and fall. It is possible that the steering flow will be modified to use an average over altitudes between 2.5-5 km). In regions where a valid TITAN vector exists, the RUC wind is replaced by the TITAN motion. The TITAN motion populates the grid within a 100 km radius of the storm. If there is an overlap between TITAN vectors, a distance weighted average value is used.

In the second step, the motion vectors are forced to be within 5 km/hr or 20° of the previous vector at a given grid point. This forces the transition between RUC and TITAN vectors to be smooth and acts to stabilize the motions. These motion vectors are used along with the NCWF-2 to calculate probabilities.

#### c) Probabilities

The NCWF-2 methodology used to calculate the first guess probability field is described in Germann and Zawadzki (2004, referred to as GZ). GZ suggest that a straight forward way to determine probabilities is to determine the spatial distribution of the data in the neighborhood of the point of interest. They suggest four ways to calculate probability distributions. The Synoptic Eulerian (called SE) calculates the Probability Distribution Function (PDF) based on the reflectivity distribution across the entire radar mosaic. The Local Eulerian (LE) determines PDF based on the reflectivity distribution locally around a point with no motion applied. The Local Lagrangian (LL) calculates the PDF based on the reflectivity distribution locally around a point after adjusting for storm motion. The Conditional Lagrangian Mean (CLM) calculates the PDF based on the reflectivity distribution within an area of smoothed reflectivity with the same value as extrapolation forecast. GZ uses statistical validation to conclude that the LL technique provides the best results.

An example of the LL technique is shown in Fig. 8. Figures 8a and b illustrate the processing steps for determining probability based on GZ's Local Lagrangian technique and Figs. c and d show the NCWF-2 probabilities. As in GZ, reflectivities are used to illustrate the LL technique. The yellow/brown colors in Figs. a, c, and d indicate reflectivity values. The probability distribution shown in Fig 8b is the forecast for a point P (shown in Figs. 8a, c, and d). The arrow in Figs. 8a, c, and d indicates the trajectory

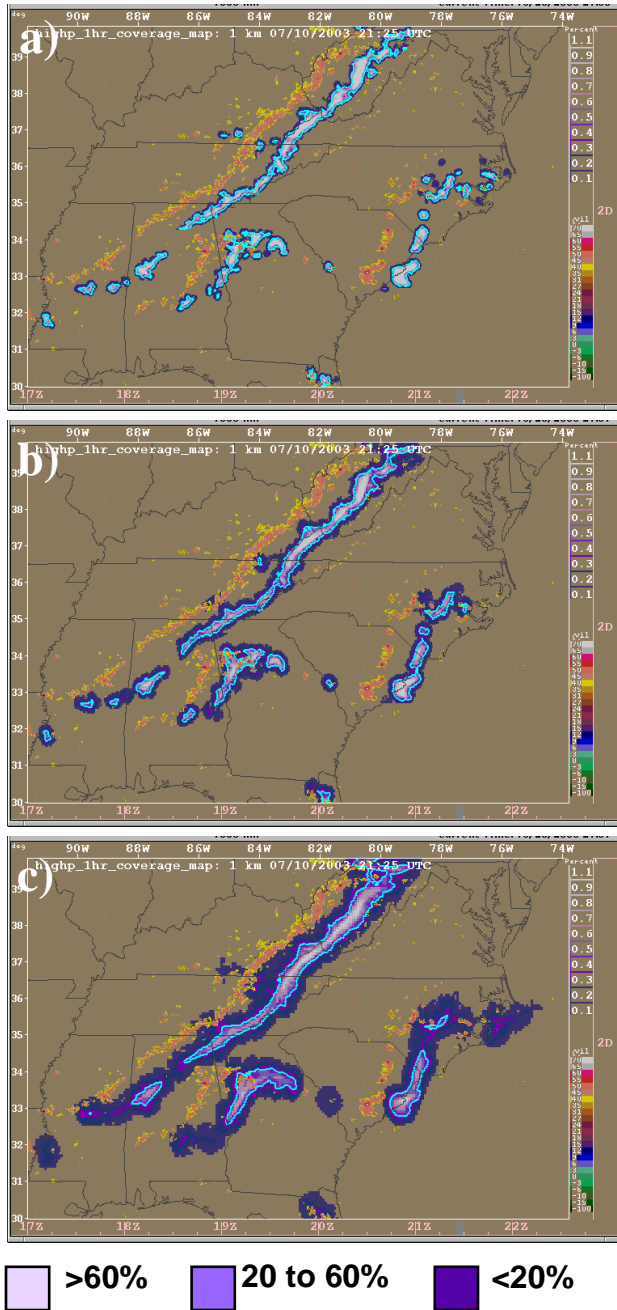


Figure 9. Shows example probability fields based on a scale of 30 km (a), 60 km (b), and 120 km (c). The 40% contour is shown as the cyan overlay. The yellow and red overlay is the NCWD level 3 and above.

based on storm motion that is followed back to its origin to determine the PDF. The spatial distribution (probability) of storms is determined for point P within a region encompassed by the

white circle of diameter  $k$  shown in Figs. 8a, c, and d. Figures 8c and d indicate a field of probabilities in shades of purple which are determined for a single threshold level shown as the dashed line in Fig. 8b for a reflectivity value of 40 dBZ. The probability field is calculated based on conditions at forecast time (Fig 8c) and advected based on the NCWF-2 motion vectors. One of the primary issues with this methodology is determining the optimal scale,  $k$ , for calculating the PDF (the diameter of the circle).

GZ calculates that the optimal scale based on the full PDF (as shown in Fig. 8b) is approximately 1 km per min ( $k=60$  km for a 60 min forecast) based on evaluations using the Conditional Square-root of the Ranked Probability score. For NCWF-2, a full probability density function at each point is not desirable. Instead, a binary-NCWD field is used for calculating the probabilities. Probabilities are calculated by determining the area coverage of convection within an elliptical region. An ellipse is used instead of the circle suggested by GZ because it maintains linear features. The elliptical region is rotated at 10 degree intervals to determine the orientation with the maximum area coverage. The maximum area coverage is mapped as the probability level (purple shades in Fig. 9). Probabilities are extrapolated based on the storm motion vector field discussed in Section 2b.

Figure 9 illustrates the effect of the scale on LL probabilities. The probabilities (shown in Figs 9a, b, and c) are calculated using ellipsoids of 30x8, 60x16, and 120 x 32 km (or scale of 30, 60, and 120 km respectively). As expected, the smaller scale retains the structure of the convection and has more high level (light color) probabilities. The larger scales smooth out much of the convective structure and have fewer high probability regions. As a test of forecast scale, reliability charts are shown Fig. 10. Two convectively active 24 hr periods were evaluated. The first started at 12Z on July 10, 2003 (shown as the left hand column of Fig. 10) and the second started at 15Z (shown as the right hand column of Fig. 10). Probability forecasts for 15, 30, 45, 60, 75, 90, 120 and 180 minutes are shown. The plots are based on a grid-to-grid comparison of the forecast and observed fields. The observations and forecasts are extended 10 km in order to relax the stringent requirements of the grid-to-grid comparisons. A perfectly reliable forecast would fall along the purple diagonal lines shown in Fig. 10. These plots are encouraging because they show that using a spatial filter to derive probabilities provides reliable forecasts. Further work is needed to better understand and calibrate the probabilities. Additional data sets should be evaluated and data needs to be stratified based on convective organization.

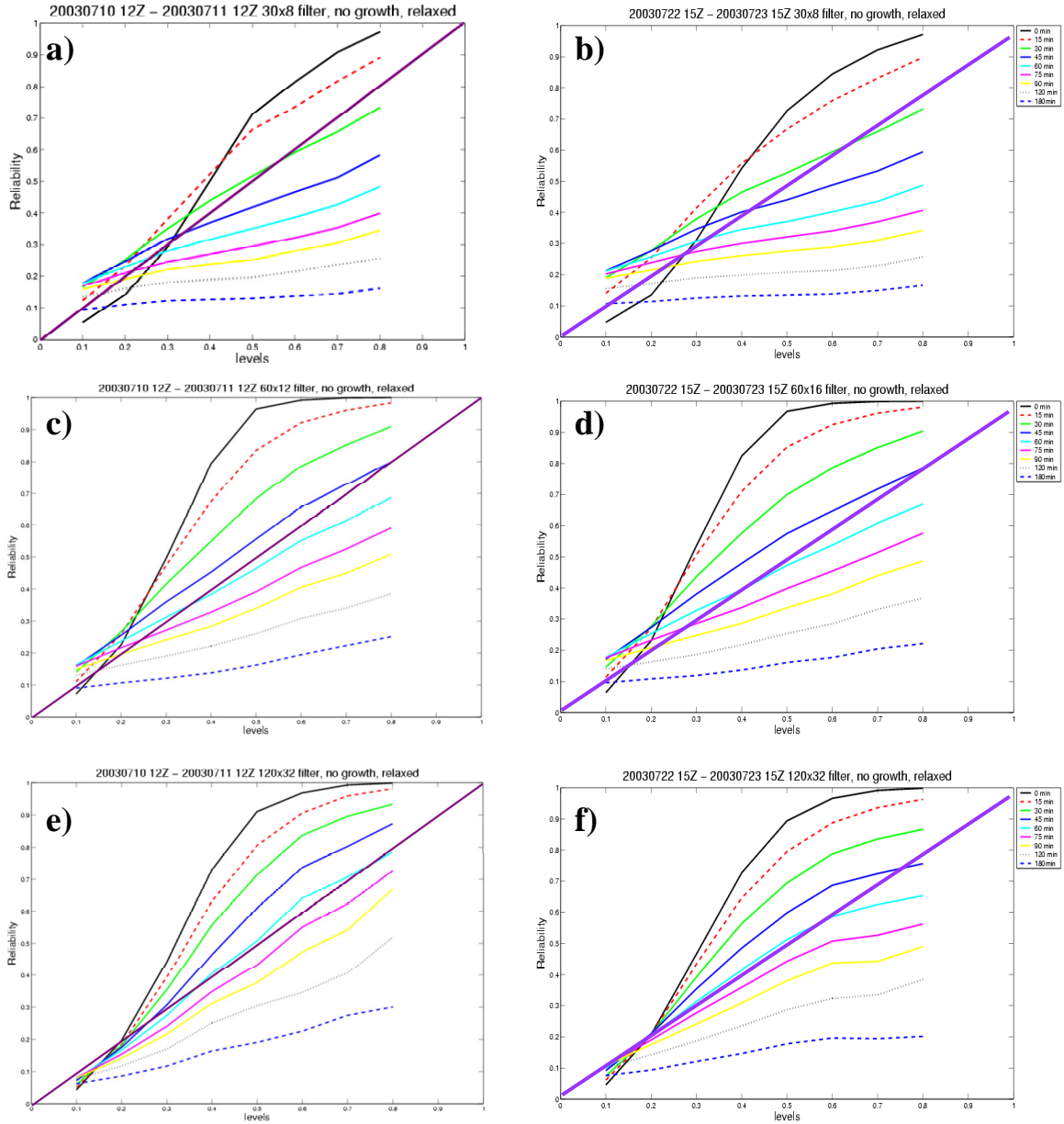


Figure 10. Reliability plots for two convectively active 24 hr periods are shown; the first started at 12Z on July 10, 2003 (a, c, and e) and the second started at 15Z (b, d, and f). Forecast scales are 30 km (a and b), 60 km (c and d), and 120 km (e and f). Probability forecasts for 0 (black solid line), 15 (red dashed), 30 (lime green solid line), 45 (dark blue solid line), 60 (cyan solid line), 75 (magenta solid line), 90 (yellow line), 120 (gray solid line) and 180 (blue dashed line) minutes are shown. A perfectly reliable forecast would fall along the diagonal purple line.

However, based on these plots, GZ's recommendations, and further analysis by RTVS, a filter size of 60 km and 120 km is used for the 1 and 2 hr NCWF forecasts, respectively.

*d) Modification of probabilities based on trending dissipation*

Tsonis and Austin (1981) first investigated the use of trends in echo size and intensity to improve forecasts out to 30 min. Trending was further tested by Wilson et al. (1998) using TITAN

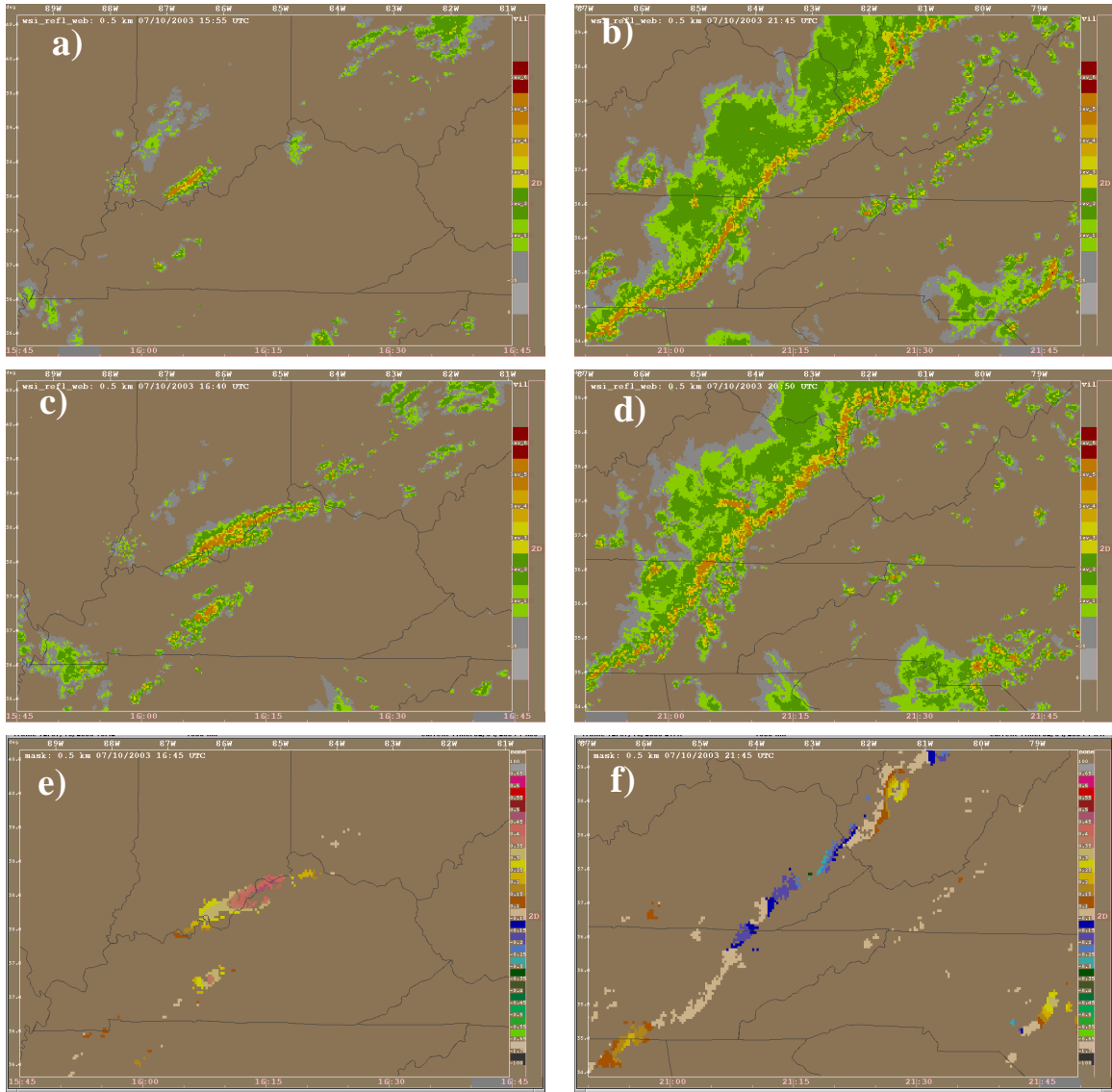


Figure 11. Two cases, growth (a, c, and e) and dissipation (b, d, and f) are shown. (a), (b), (c), and (d) are the NCWF field. The data shown in (c) and (d) are one hour later than the data shown in (a) and (b) respectively. (e) and (f) show trends. Yellows and reds indicate regions of growth and blues and greens regions of dissipation.

for forecasts ranging between 6 and 36 min. In both cases, little if any improvement was found. Wilson et al. (1998) concluded that “essential physical processes that dictate the change in rainfall with time are not necessarily observable in the past history of a particular echo development.” However, in an analysis of 0-2 hr forecasts, Boldi et al. (2003) suggest that trending provides benefit. The difference in these studies is one of scale. In the earlier studies, individual cells were tracked and trended. In the Boldi et al. (2003) work, the area change of the

region around an individual grid point was evaluated. Instead of evaluating whether an individual cell was growing or dissipating, all the cells within a region were examined.

The NCWF-2 provides trending information for display and uses the dissipation rate in the forecasts. Examples of growth and dissipation are shown in Fig. 11. NCWF-2 trends are calculated (Rehak et. al. 2004) in Lagrangian space (based on motion vectors at forecast time). The trends are calculated based on a weighted

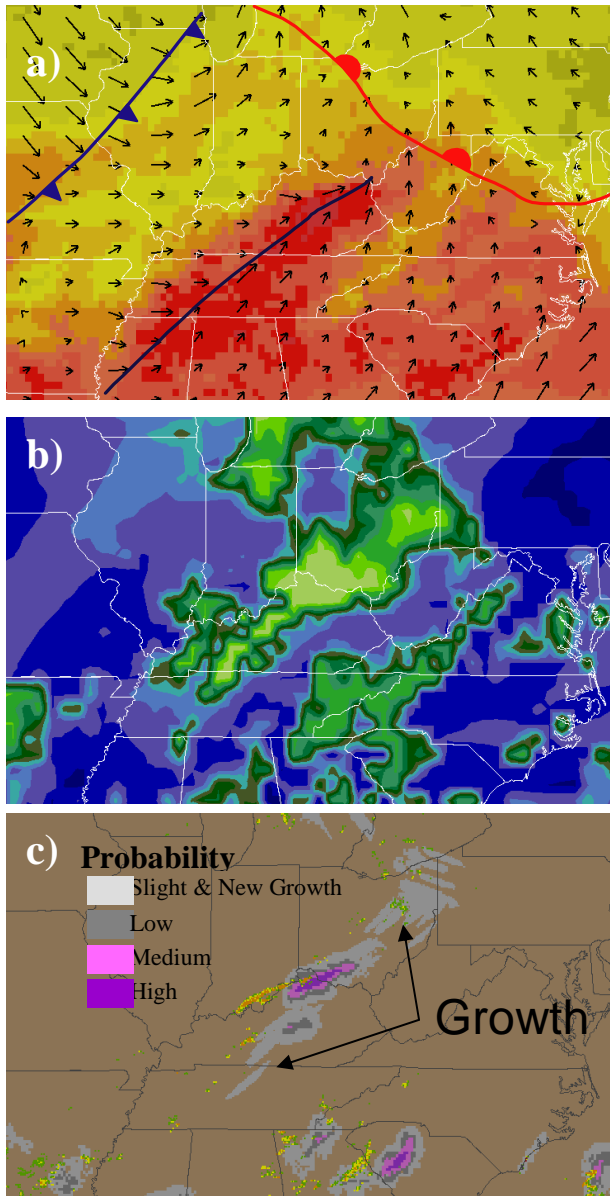


Figure 12. Example of how the RUC data are used for adding regions of low probability. (a) shows the RUC analysis of  $\Theta_e$  and low level winds (black vectors). The boundaries are from the NWS-HPC. (b) shows the convective potential field (see text) on this field. The light green color indicates the area that has the highest potential for storm development and the blue colors indicate the least potential. The corresponding 2-hr forecast is shown in (c). Low probability growth forecasts are orientated in the direction of the large-scale forcing.

linear fit of the mean probability within an 80 km diameter circle over an hour period. Only dissipation trends are used to modify probability forecasts.

*e) Addition of low probability nowcasts in regions of RUC-detected large-scale forcing and instability*

RUC analyses and forecasts are used to assess the potential for development and growth of deep convection over a 0-2 h period. This information is used along with the presence of small storms (50-300 km<sup>2</sup>) to add low-probability nowcasts in regions of potential storm development. The RUC based algorithm uses fuzzy logic to combine convective available potential energy (CAPE) and convective inhibition energy (CIN) at 25 mb levels through boundary-layer, temperature advection (theta-e advection), relative humidity, shear, RUC forecasted convective precipitation, and a large-scale forcing field called Convective Potential. The large-scale forcing field or frontal likelihood is based on the gradient in low-level potential temperature, vorticity, and convergence, and is used to determine the orientation of large-scale frontal forcing. A climatology based on national composites of radar reflectivity for the past eight warm seasons (1996-2003) is used to help determine regions of growth. Appendix 1 has detailed information on these fields and how they are calculated.

Figure 12 provides an example of how the RUC data are used for adding regions of low probability. Figure 12a show the RUC analysis of equivalent potential temperature and low level winds (black vectors). The boundaries are from the NWS-HPC. Figure 12b shows the convective potential field. The light green color indicates the areas that have the highest potential for storm development during the two hour period and the blue color indicates the least potential. The corresponding 2-hr forecast is shown in Fig. 12 c. In regions where the convective potential field indicates potential for convective development, climatology is favorable, and there are small storms already beginning to form, a low probability forecast is entered in the orientation of the large-scale forcing.

### 3. Displays

The displays shown in Figs. 13, 14, and 15 for both ADDS and NWS-NAWIPS are considered first drafts. Generally, the look and feel of the display can be modified to meet user needs. These are offered as suggestions and will most likely be changed.

*Display on ADDS for Aviation Users*

Example ADDS displays are shown in Figs 13 and 14. Figure 13 shows the proposed mapping of the probability levels in shades of gray and purple. These colors differentiate between radar observations and forecasts. Allowing the user to visualize the quality of the current forecast is always a priority. A draft product performance diagram is shown in Fig. 14 where the binary-NCWD (red) is super-positioned on the forecast.

*Display on NAWIPS for AWC forecasters*

A long term goal for NCWF is to move toward a

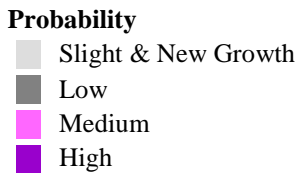
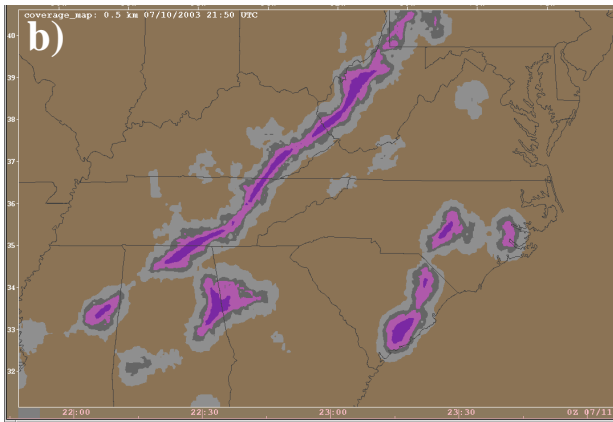
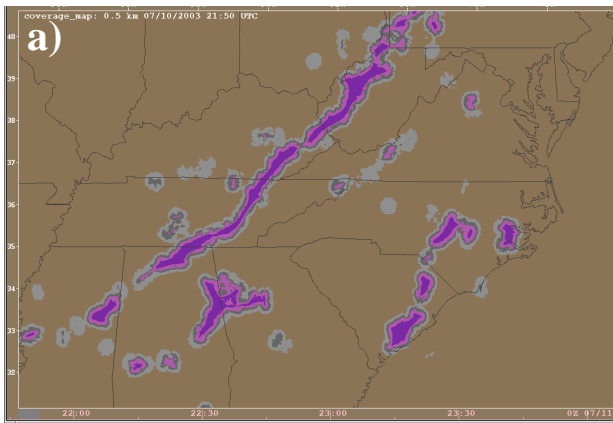


Figure 13. Example forecasts for 1hr (a) and 2hr (b).

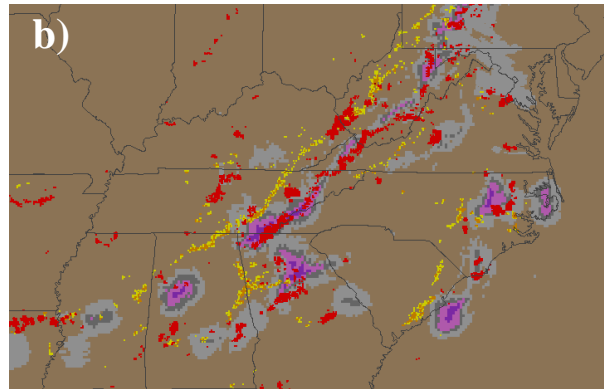
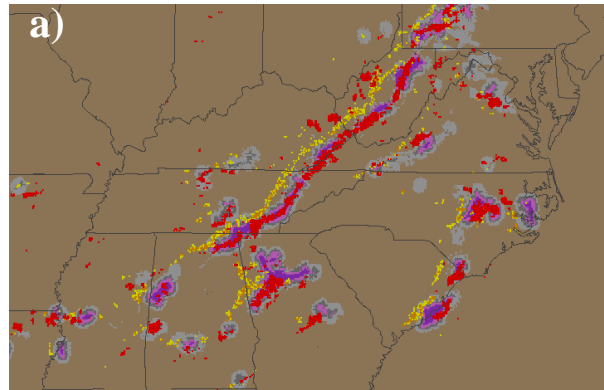
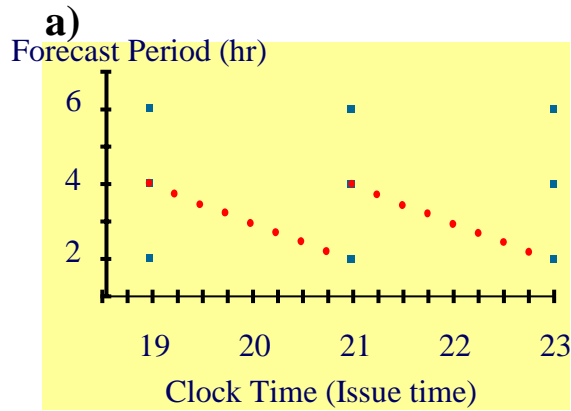


Figure 14. Example forecast performance graphs for forecasts shown in Fig. 13. The forecasts are 1hr (a) and 2hr (b). The red overlay is the binary-NCWD at the validation time.

continuous 0-6 hr forecast. In the near-term, a 0-6 hr NCWF will most likely combine output from NWP (RUC), observation-based systems (NCWF-2) and a forecaster. The advantage of this methodology is that it utilizes the strengths of each component. As a starting point toward this collaboration, NCWF-2 will be displayed on the AWC forecasters NAWIPS display. The display will be tailored to match the CCFP forecaster forecast cycle. The CCFP forecasts are for 2, 4, and 6 hr. Forecasts are issued every other hour (illustrated as blue boxes in Fig. 15). The NAWIPS-NCWF would be issued at the time and over the forecast period indicated by the red boxes. So, at 19Z, a 4 hr forecast is issued, at 19:15Z a 3hr 45min forecast is issued, et cetera. Although these longer period forecasts are not



Issued – 07/10/03 22:45, Valid – 07/11/03 01:00, FT = 135 min

Figure 15. (a) forecast time line for the CCFP and NAWIPS-NCWF is shown. The CCFP forecasts are represented as blue boxes 2, 4, and 6hr forecasts are issued every other hour. The NAWIPS-NCWF would be issued at the time and over the forecast period indicated by the red boxes. At 19Z a 4hr forecast is issued, at 19:15Z a 3hr 45min forecast is issued, et cetera. (b) is the NAWIPS-NCWF display where forecasts are over-layed in gray and purple contours that represent probability levels shown in Fig. 13 on any base field [(b) shows NCWD].

ready for non-meteorologists, they could prove useful to the forecaster because the automated extrapolations free the forecaster to focus on areas of initiation, growth and decay.

#### 4. Discussion

This paper documents the NCWF-2 system that was implemented at the Aviation Weather Center (AWC) this summer. Validation statistics are provided in the corresponding AWRP Quality Assessment group paper. Running NCWF-2 at the AWC this summer is an important first step in developing a four-way collaboration between NCAR, MIT/LL, FSL/RUC, and AWC. Hopefully,

this collaboration will lead to a continuous 0-6 hr forecast. In addition, user exposure through experimental ADDS to probabilistic forecasts will act as a starting point towards defining requirements for the NCWF-2 or successor system and concepts of use.

### Appendix 1: Analysis of RUC-II Outputs and Precipitation Climatology Information for use in the NCWF-2

#### 1. Background

Traditional approaches to nowcasts (0-3 hr forecasts) of deep convection have typically used extrapolation and trending of remotely sensed (e.g., radar, satellite) storms. However, the environment of deep convection and the internal dynamics of the convection itself can evolve significantly over the nowcasting period, which represents a limitation of this approach. Recent efforts in short-term numerical weather prediction (NWP) at cloud resolving resolutions have provided a promising alternative or supplemental approach to traditional methods based on extrapolation of observations. However, high-resolution deterministic NWP is currently prohibitively expensive for operational applications and is also exposed to various uncertainties in subgrid physical parameterizations and data assimilation. Current operational models (e.g., NCEP's ETA and RUC-II models), while of insufficient resolution to simulate convective storm cells, nevertheless provide several types of useful information that can supplement traditional nowcasting approaches. In the current approach, we use both mesoscale ( $L \geq 100$  km) diagnostics derived from operational RUC-II model analyses and forecasts and short-term (0-3 hr) RUC-II quantitative precipitation forecasts to determine where pre-existing deep convection is most likely to experience real growth.

An environmental characteristic of first order importance for both the development and sustenance of deep convection is the thermodynamic stability. Two critical measures that characterize the thermodynamic stability are the CAPE and the CIN. The CAPE for a hypothetical air parcel is defined as the vertically integrated positive buoyancy between its level of free convection (LFC) and its equilibrium level where it ceases to be positively buoyant with respect to its environment. The CIN is a measure of the vertically integrated negative buoyancy between the source region of the air parcel and its LFC.

Figure 16a illustrates the regions of CIN and CAPE for a surface-based air parcel in a

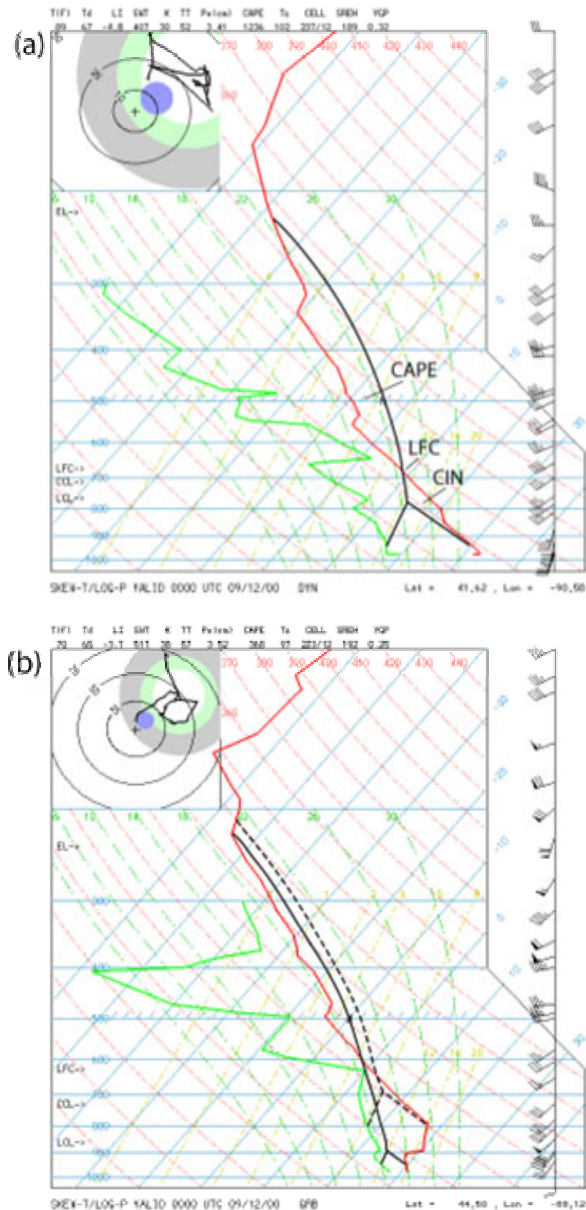


Figure 16. SkewT-lnP diagrams of temperature and moisture at 0000 UTC 11 September 2000 for locations (a) ahead of a cold front where the most thermodynamically unstable air is situated within the boundary layer and (b) north of rain-cooled convective outflow where the most thermodynamically unstable air is situated above the boundary layer. In both panels hypothetical air parcel ascent curves are in black and vertical profiles of environmental temperature and dewpoint are in red and green, respectively. See text for additional discussion.

conditionally unstable environment. This particular sounding is susceptible to deep convection provided the CIN [negative buoyancy resulting from environmental virtual temperature (red curve) excess over that of the air parcel (black curve)] can be overcome either by surface heating or mechanical lifting. For daytime soundings within a heated boundary layer (Fig. 16a), air parcels originating near the surface have the largest CAPE. Locations that possess relatively stable boundary layers, such as those that have experienced strong nocturnal cooling or those which exist on the cool side of shallow surface frontal boundaries, may also be susceptible to deep convection provided that conditional instability exists above the surface-based cool layer. Figure 16b presents such a sounding where an air parcel originating ~ 2 km above the surface at 800 mb (dashed black curves) is more thermodynamically unstable (i.e., has larger CAPE and smaller CIN) than conditions near the surface (black solid curves), which in this particular example had experienced cooling from recent thunderstorm activity.

## 2. An algorithm for convective potential based on RUC thermodynamic conditions

It is clear from the example presented in Fig. 16 that a comprehensive analysis of thermodynamic stability needs to account for the stability of the air originating not only in the boundary layer, but throughout the entire depth of the lower troposphere. We now describe an algorithm that assesses susceptibility to deep convection based on the depth of the lower-tropospheric layer that possesses significant thermodynamic instability. Analyses of convective precipitation have indicated that given a reasonable threshold value of instability is exceeded, the depth of the thermodynamically unstable layer may be a more useful indicator of whether mesoscale regions of convection will develop or be sustained than the actual magnitude of the maximum instability. This is consistent with the idea that deep lower-tropospheric layers that are thermodynamically unstable (i.e., have significant CAPE with small values of CIN) are often generated in part by atmospheric forcing favorable for deep convection, such as organized upward motion. The algorithm inputs gridded three-dimensional RUC-II pressure-level data and outputs a two-dimensional (i.e., horizontal) field that approximates the "depth" of thermodynamic instability and consists of the following three basic steps

- 1) At each RUC vertical grid point (i.e., every 25 mb) it is determined if both  $CAPE \geq 500 \text{ J/kg} + \delta$  (Relative Humidity) +  $\delta$  (Advective Forcing)

## Modification to CAPE/CIN Thresholds by $\delta(x,y)$ Correction Terms

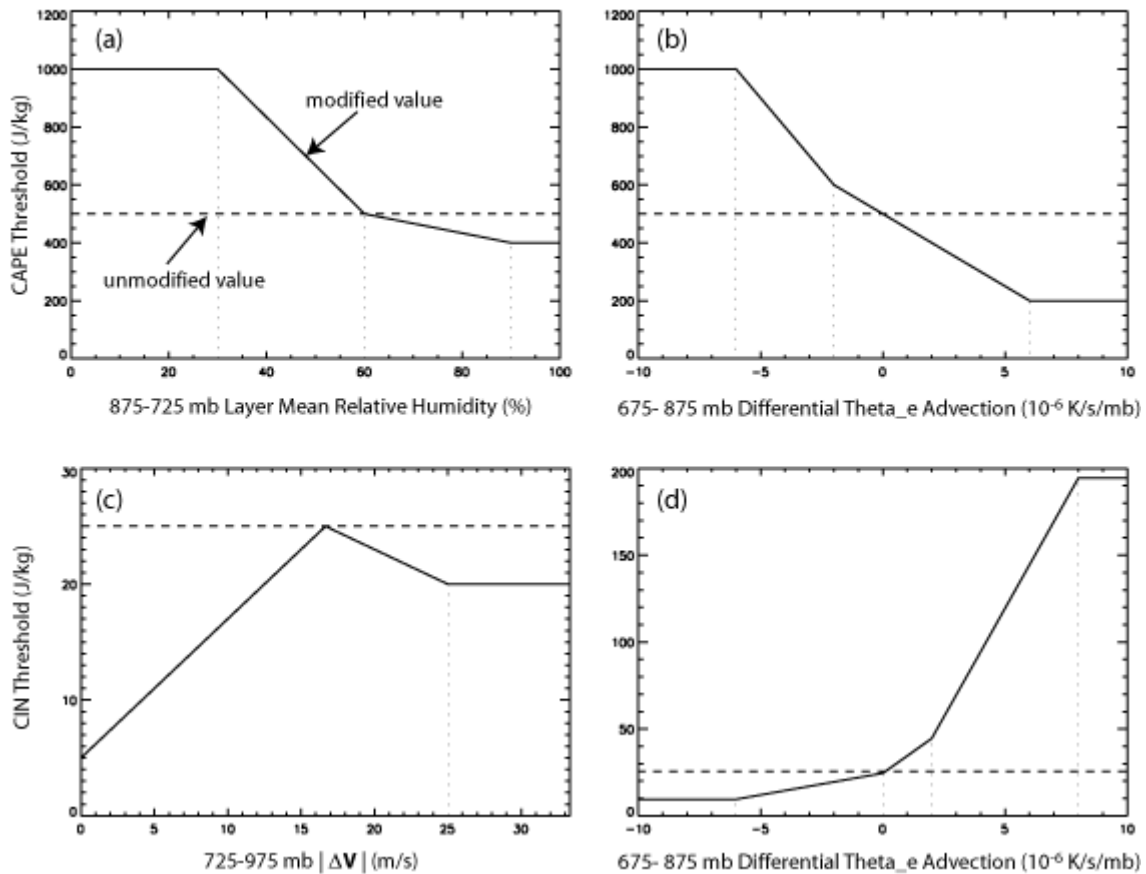


Figure 17. Modification to the (a and b) CAPE threshold (green) and (c and d) CIN threshold (red) for counting of thermodynamically unstable levels by the two-dimensional correction terms discussed in the text. The unmodified values of the (a and b) CAPE and (c and d) CIN thresholds are represented by the black dashed lines.

$CIN \leq 25 \text{ J/kg} + \delta(\text{Vertical Shear}) + \delta(\text{Advective Forcing})$ , where the  $\delta(x,y)$  are two-dimensional corrections based on layer averages or differences.

- 2) Assign grid point values based on whether the above criteria are satisfied YES: Value = 1.0 (isolated) or = 1.5 (vertically juxtaposed to similar point) NO: Value = 0
- 3) Sum grid point values in each vertical column to produce the two-dimensional field called `vert_sum_interest`.

The threshold values for CAPE and CIN in step (1) are based on physical considerations and case studies of outbreaks of mesoscale

convection from the 2000 warm season. Figure 17 illustrates how the two-dimensional correction terms modify the CAPE and CIN thresholds. For example, we employ a base threshold for CAPE of 500 J/kg at each vertical grid point, which is modified by the lower-tropospheric relative humidity (Fig. 17a) and differential advection of equivalent potential temperature (Fig. 17b). In dry environments, entrainment will have a more deleterious effect on actual air parcel buoyancies in convection than in moist environments. This is the rationale behind requiring CAPE to be larger ( $\geq 1000 \text{ J/kg}$  when  $RH \leq 30\%$ ) under dry conditions and similarly relaxing this criterion ( $\geq 400 \text{ J/kg}$  when  $RH \geq 90\%$ ) for very moist conditions (Fig. 17a). Differential advection of equivalent potential temperature,  $\Theta_e$ , is capable of causing dramatic changes in CAPE and CIN, which can affect environmental

thermodynamic instability on 1-3 hr nowcast timescales and is used as a dynamic correction for current RUC analyses (Figs. 17b,d). The relatively minor vertical shear correction to the

CIN threshold (Fig. 17c) is based on the notion that deep convection has difficulty organizing into mesoscale structures at low shear values, whereas when the shear is too strong, initiation of convection is more difficult.

The correction terms for the CAPE and CIN thresholds are additive and their combined effect on thresholds are summarized in Fig. 18. The CAPE threshold value (Fig. 18a) may be less than 200 J/kg when conditions are both moist

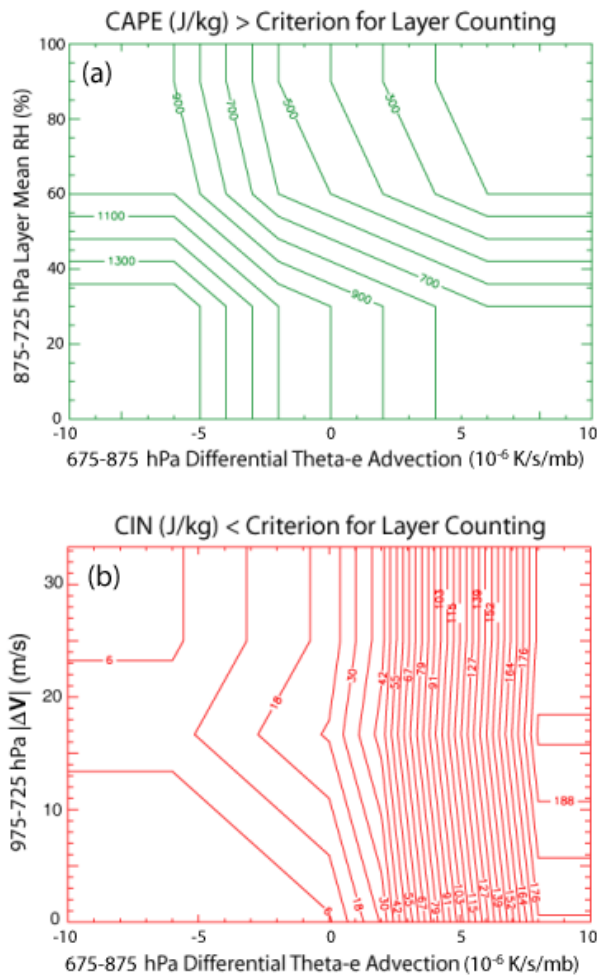


Figure 18. Combined effect of both two-dimensional correction terms on thermodynamically unstable layer (level) counting criteria for (a) CAPE and (b) CIN. See text for additional discussion.



Figure 19. Contours of *vert\_sum\_interest* in intervals of 4 (25-mb vertical layers) and observed VIL (vertically integrated liquid water) ~ 2 hr later on 22 August 2000.

and likely to be rapidly destabilizing due to greater positive advection of warm, moist air near the top of the boundary layer than in the middle troposphere. By contrast, under less favorable conditions of differential advection coupled with low relative humidity, CAPE is required to approach 1500 J/kg. Similarly, Fig. 18b illustrates how significant CIN is allowed under conditions of favorable differential  $\theta_e$  advection, whereas very small values of CIN are required when this parameter is unfavorable. The small modification due to the vertical shear conditions are most noticeable under the latter condition.

In step (2), vertical levels that satisfy the step (1) criteria and are adjacent to similar thermodynamically unstable vertical levels are given greater weight (1.5) than isolated (1.0) thermodynamically unstable levels. This is because a single deep layer of instability, in most instances, is more conducive to deep convection than several shallow layers of instability that are separated by some distance in the vertical. In the final step (3), the values for all 13 levels in the 1000 to 700 mb vertical column are summed at individual horizontal locations to produce the two-dimensional *vert\_sum\_interest* field. An example of the *vert\_sum\_interest* field and its association with precipitation ~ 2 hrs later is shown in Fig. 19.

### 3. Real-time estimation of *vert\_sum\_interest*

Although the calculation of *vert\_sum\_interest* is straightforward, there are significant considerations involved in its successful implementation in a real-time operational setting. One obstacle is the delay involved in acquisition and processing of the RUC analysis fields. Typically, the most recent RUC analysis will be 1 hr old by the time it is acquired and processed, which is undesirable for use in a 0-3 hr (short-

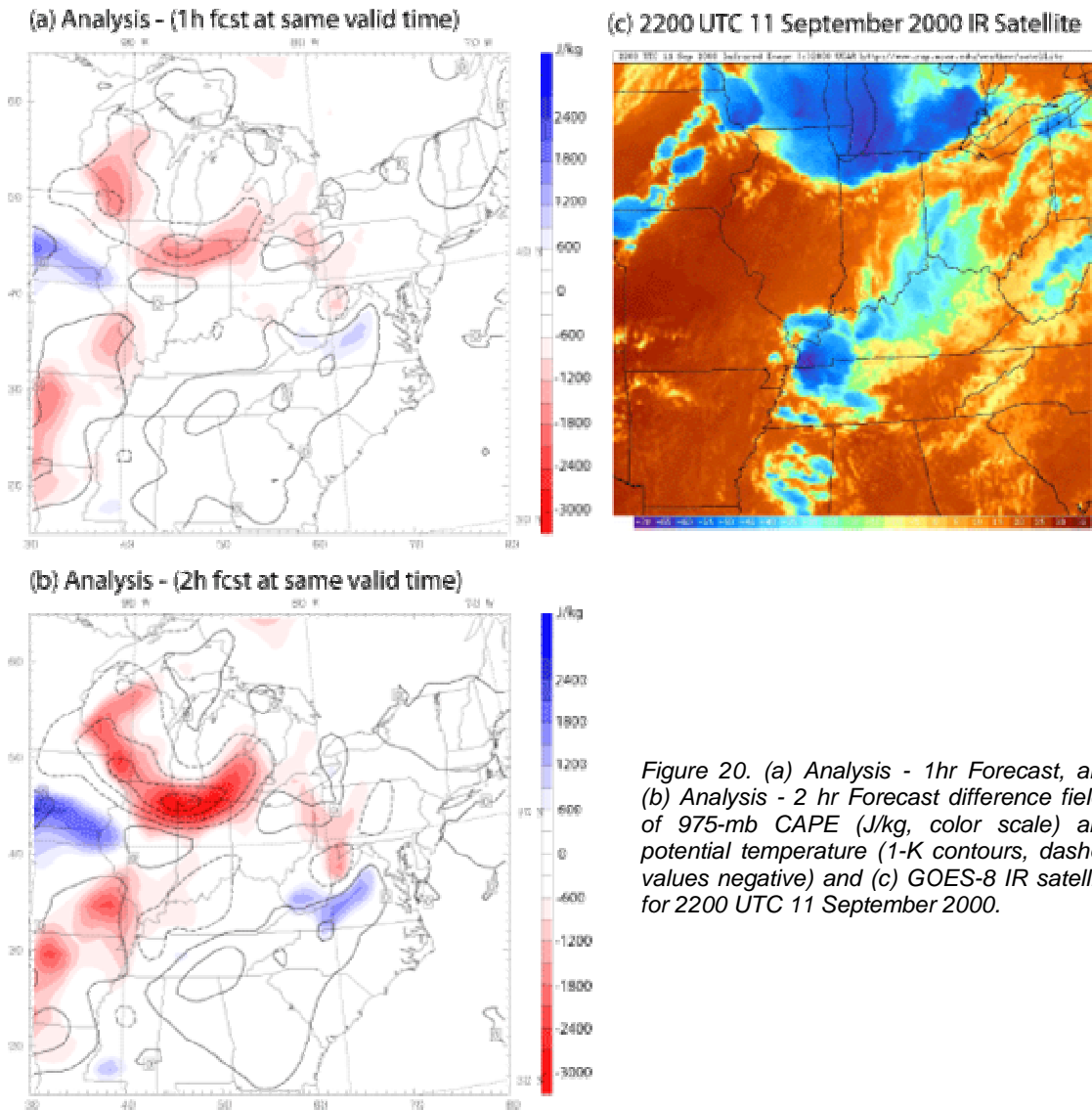


Figure 20. (a) Analysis - 1hr Forecast, and (b) Analysis - 2 hr Forecast difference fields of 975-mb CAPE (J/kg, color scale) and potential temperature (1-K contours, dashed values negative) and (c) GOES-8 IR satellite for 2200 UTC 11 September 2000.

range) convection forecast. It is thus necessary to obtain an estimate of the future analysis that corresponds to atmospheric state for the actual time that the calculation of `vert_sum_interest` is intended to represent.

Short-term (1-2 hr) RUC forecasts from the same forecast cycle are a possible candidate for use in the calculation of `vert_sum_interest`. The use of forecasts would not be sensitive to the aforementioned delays, and would also provide information on the possible future state of the atmosphere that could be useful for forecasting evolution of deep convection. However, in tests applied to convection cases during the 2000 warm-season, we found significant departures between CAPE/CIN values derived from

analyses and forecasts valid at the same time as the analyses.

Figure 20 illustrates the departures in the short-term RUC 1000 mb CAPE (colors) and potential temperature fields (contours) for an example case. Here, the model CAPE errors (Figs.20 a,b) are greatest in the vicinity of a large convective system in the upper Midwest (Fig. 20c) and increase with the length of the forecast (compare Figs. 20a and 20b). This type of CAPE error is due to model temperatures being too warm at low-levels in the vicinity of the observed convective system which likely results from the inability of the model to produce deep convection rapidly enough to sustain the preexisting (observed) low-level cold pool.

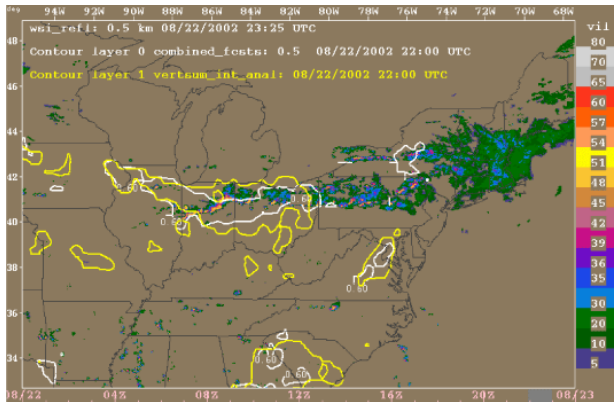


Figure 21. 0.6 interest value contour for  $f(\text{vert\_sum\_interest})$  (yellow) and Convective Potential (white), each lagged 85 minutes from the overlaid reflectivity field on 22 August 2002.

This particular type of temperature error was generally restricted to the lowest 100 mb of the troposphere. However, it was commonly observed in the vicinity of convection and occurred in the portion of the troposphere where CAPE is most sensitive, which makes it undesirable to estimate a future analysis based solely on 1 or 2 hr forecasts. Through statistical analysis of several case studies, it was found that CAPE and CIN averages of the most recent analysis and the latest 1-hr forecast from the same RUC forecast cycle produced the most accurate estimates of CAPE and CIN for the future analysis time. Using an extrapolated analysis (i.e., the most recent analysis + the trend between the two most recent analyses), in place of the most recent analysis, when averaged with the 1-hr forecasts produced comparable results and had the desirable property of each component of the two-member ensemble (i.e., the 1-hr forecast and the extrapolated analysis) being valid at the identical time which is  $t = 1$  hr after the most recent available analysis. Thus, we estimate the three-dimensional fields of CAPE and CIN used in the calculation of  $\text{vert\_sum\_interest}$  as follows:

$$F_{1,*} = [F_{0,1} + F_{0,0} + (F_{0,0} - F_{-1,0})]/2,$$

where  $F_{ij}$  are the  $j$ th hour forecasts of CAPE/CIN from the  $i$ th hour RUC cycle. The terms on the right side of the equation,  $F_{0,1}$ ,  $F_{0,0}$ , and  $F_{0,0} - F_{-1,0}$  correspond to the most recent 1-hr RUC forecast, the most recent analysis, and the analysis trend, respectively. The two-dimensional fields of differential  $\Theta_{e}$  advection, layer-averaged relative humidity, and vertical shear used to modify the local CAPE/CIN thresholds discussed

in section 2 are estimated using only the most recent 1-hr RUC forecast:

$$F_{1,*} = F_{0,1},$$

since these quantities are computed using layer averages (relative humidity) or differences ( $\Theta_{e}$  advection, vertical shear) taken above the surface, where the 1-hr RUC forecasts were more consistent with the analyses.

#### 4. The Convective Potential Field

Examination of  $\text{vert\_sum\_interest}$  using both statistics for the entire 2003 warm season and subjective examination for 4 case studies of diverse widespread convective events during the 2002 warm season revealed that while it often provided reasonable guidance of where mesoscale convection was likely to be present over the subsequent 0-3hr, it produced an unacceptably large false alarm rate in some cases. To mitigate this deficiency  $\text{vert\_sum\_interest}$  was combined with RUC 3-hr precipitation amount forecasts directly output from the model and the  $\text{filtered\_lik}$  field derived from model output. The RUC 3-hr precipitation forecasts have significantly advanced in recent years due in part to improvements in the convection parameterization schemes used in the model. A large false alarm rate also occurs with this product; however, false alarms from  $\text{vert\_sum\_interest}$  and the RUC 3-hr precipitation forecasts are not always well correlated. Thus, by using both fields the false alarm rate could be reduced somewhat. The  $\text{filtered\_lik}$  field is designed to identify meso-synoptic ( $L = 100\text{-}1000$  km) frontal structures based on vertical vorticity, horizontal divergence and horizontal gradients of  $\Theta_{e}$ . By itself, this field tends to identify horizontal scales that are significantly greater than those over which the organized convection occurs. However, it does provide important information on large-scale forcing that helps support the mesoscale organization of convection, which  $\text{vert\_sum\_interest}$  is not always able to provide.

A new two-dimensional interest field,  $\text{Convective\_potential}$  is defined based on a combination of  $\text{vert\_sum\_interest}$ ,  $\text{ruc\_precip}$ , and  $\text{frontal\_likelihood}$  ( $\text{frontal\_likelihood}$  is based on low-level gradient of  $\Theta_{e}$ , vorticity, and convergence). Figure 21 shows the association of precipitation with regions where  $\text{Convective\_potential} \geq 0.6$  (white contours) and  $f(\text{vert\_sum\_interest}) \geq 0.6$  (yellow contours). Here, a linear band of deep convection is oriented west-east along a frontal zone from western Indiana into Pennsylvania and upstate New York. Both  $\text{vert\_sum\_interest}$  and  $\text{Convective\_potential}$  are able to capture the region of most intense and contiguous convection that occurred 90-min later in Indiana and western

Ohio. At this 0.6 threshold, neither interest field is well correlated with the less widespread strong ( $\geq 40$  dBz) convection, farther east along the band, though Convective\_potential at least hints at its presence (both fields are able to detect much of this convection at lower threshold values). Outside of this zone of linear convection, from combining the `ruc_precip` and `filtered_lik` with `vert_sum_interest`, it is clear that Convective\_potential has a better false alarm rate than using `vert_interest` alone in this example.

#### 5. Use of diurnal rainfall climatology

In many locations, the frequency of precipitation is closely tied to the diurnal cycle. The phase and amplitude of this pattern differs from region to region due to factors such as physiography, latitude, and average humidity. In general, the diurnal signal is strongest during the warm season over land as radiative forcing modulates the convective available potential energy (i.e., it rains during the day in the summer). Regular mesoscale circulations due to land/sea breezes or mountain-valley flows also augment the local diurnal signal.

To take advantage of the potential predictive value inherent in regional diurnal variations in rainfall probability as suggested by Boldi (2000), an eight-season climatology of radar echo frequency was compiled over the U.S. according to time of day. The NOWrad MASTER15 product produced by WSI Corporation was the data source used for the climatology. Every fifteen minutes, WSI combined radar reflectivity volumes from all WSR-88D radars into a national composite on a  $2 \times 2$  km<sup>2</sup> grid. The final product comprised the highest reflectivity in a vertical column and was rounded to the nearest 5 dBZ. The frequency of  $\geq 40$  dBZ reflectivity was recorded at each grid point for all times between 1 June 0000 UTC and 31 August 2345 UTC for the 1996-2003 seasons. The fifteen minute products were grouped into hours such that 0200 UTC consisted of all 0145, 0200, 0215, and 0230 UTC products. Using the standard reflectivity-rainfall rate (Z-R) relationship employed by the National Weather Service ( $Z=300R^{1.4}$ ), 40 dBZ corresponds to about 12 mm/hr.

The mean hourly rate of change of precipitation likelihood (`dfreq40`, in fraction per hour) is a smoothed field - both in time and space. We calculate the mean hourly rate of change using a finite difference centered on each UTC hour. The 4-h window ( $t+2hr - t-2hr$ ) smooths random hourly fluctuations and produces a steady signal. The  $2 \times 2$  km<sup>2</sup> data was spatially averaged with a  $9 \times 9$  grid point box filter, and then resampled at 10 km grid spacing.

In NCWF-2 storm cells are eligible for growth (see Section 2e for details) when they 1) meet specified size criteria, 2) are not embedded within a large mass of stratiform precipitation, 3) the Convective\_potential field (previous section) exceeds a specified threshold value within a specified distance of the cell, and 4) the climatology of the diurnal cycle of precipitation does not suggest a strong probability of dissipation. If the storm cell is completely within a region of rapidly decreasing precipitation likelihood, then it is not grown. The time rate of change of precipitation likelihood (in fraction per hour) must be less than -0.0015 for this to occur, which corresponds to a limited area mostly over the southeastern U.S. for only limited hours of the day from late afternoon through early evening.

#### References

- Battan, L. J., 1959: Duration of convective radar cloud units, *Bull. Amer. Meteor. Soc.*, **34**, 227- 228.
- Bellon, A., and I. Zawadzki, 1994. Forecasting of Hourly Accumulations of Precipitation by Optimal Extrapolation of Radar Maps. *J. Hydrol.*, 157, 211-233.
- Boldi, R.A., M.M. Wolfson, R.J. Johnson Jr., K.E. Theriault, B.E. Forman, and C.A. Willson, 2002: An automated, operational two hour convective weather forecast for the corridor integrated weather. 10<sup>th</sup> Conf. On Aviation, Range, and Aerospace Meteorology, Portland, OR, 13-16 May. Amer. Met Soc., Boston, 116-199.
- Crowe, B. D. and D. W. Miller, 1999: The Benefits of Using Nexrad Vertically Integrated Liquid Water as an Aviation Weather Product. 8<sup>th</sup> Convergence on Aviation, Range, and Aerospace Meteorology, Amer. Met. Society, Dallas, TX, Pp 244-248.
- Dixon, M., and G. Wiener, 1993: TITAN: Thunderstorm identification, tracking, analysis and nowcasting - a radar-based methodology. *J. Atmos. Oceanic Tech.*, **10**, 785-797.
- Evans, J. E., and E. R. Ducot, 1994: The Integrated Terminal Weather System (ITWS). *Lincoln Lab. J.*, 7 (2), 449-474.
- Evans, J. E., K. Carusone, M. Wolfson, B. Crowe, D. Mayer, and D. Klinge-Wilson, 2002. The Corridor Integrated Weather System (CIWS). 10<sup>th</sup> Conference on Aviation, Range, and Aerospace

- Meteorology*, Amer. Met. Society, Portland, Oregon, Pp 210-215.
- Germann, Urs and I. Zawadzki, 2004. Scale Dependence of the Predictability of Precipitation for Continental Radar Images, Part II: Probability Forecasts. *J. Appl. Meteor.*, **43**, Pp 74-89..
- Hallowell, R. G., M. M. Wolfson, B. E. Forman, M. P. Moore, B. A. Crowe, T. M. Rotz, D. W. Miller, T. C. Carty, and S. F. McGettigan, 1999. The Terminal Convective Weather Forecast Demonstration. *8<sup>th</sup> Conference on Aviation, Range, and Aerospace Meteorology*, Amer. Met. Society, Dallas, TX, Pp 200-204.
- Hudson, H. R. and F. P. Foss, 2002: The Collaborative Convective Forecast Product from the Aviation Weather Center's Perspective. *10<sup>th</sup> Conference on Aviation, Range, and Aerospace Meteorology*, Amer. Met. Society, Portland, Oregon, Pp 73-76.
- Klazura, G. E., and D. A. Imy, 1993: A description of the initial set of analysis products available from the NEXRAD WSR-88D System. *Bull. Amer. Meteor. Soc.*, **74**, Pp 1293-1311.
- Robinson, M., J. E. Evans, and B. A. Crowe. En Route Weather Depiction Benefits of the Nexrad Vertically Integrated Liquid Water Product Utilized by the Corridor Integrated Weather System. *10<sup>th</sup> Conference on Aviation, Range, and Aerospace Meteorology*, Amer. Met. Society, Portland, Oregon, Pp 120-123.
- Rehak, N., D. Meigenhardt, and C.K. Mueller, "Large-Scale Trending of Radar Data" 11th Conference on Aviation, Range, and Aerospace Meteorology, Hyannis, MA, 2004
- Sherretz, L., G. Pratt, G. Thompson, and J. Henderson, 2002: Implementing ADDS Operationally at the NWS Aviation Weather Center. *10<sup>th</sup> Conference on Aviation, Range, and Aerospace Meteorology*, Amer. Met. Society, Portland, Oregon, Pp 81-84.
- Troxel, S. W. and C. D. Engholn, 1990: Vertical Reflectivity Profiles: Averaged Storm Structures and Applications to Fan-beam Radar Weather Detection in the U. S., Preprints *16<sup>th</sup> Conference on Severe Local Storms*, Kananaskis Park, Alta., Canada, Pp. 213-218.
- Tsonis, A. A., and G. L. Austin, 1981: An evaluation of extrapolation techniques for the short-term prediction of rain amounts. *Atmos.-Ocean*, **19**, 54-65
- Mahoney, J. L., J. K. Henderson, B. G. Brown, J. E. Hart, A. Loughe, C. Fischer, and B. Sigren, 2002: The Real-Time Verification System (RTVS) and Its Application to Aviation Weather Forecasts. *10<sup>th</sup> Conference on Aviation, Range, and Aerospace Meteorology*, Amer. Met. Society, Portland, Oregon, Pp 323-328.
- Megenhardt, D., C. K. Mueller, N. Rehak, and G. Cuning, 2000: Evaluation of the National Convective Weather Forecast Product. Preprints *9<sup>th</sup> Conference on Aviation, Range, and Aerospace Meteorology*, Amer. Met. Society, Orlando, Florida, Pp 171-176.
- Weber M. E., E. R. Williams, M. M. Wolfson, S. J. Goodman, 1998. An Assessment of the Operational Utility of a GOES Lightning Mapping Sensor, *Project Report NOAA-18*, MIT/Lincoln Labs.
- Wilson, J.W., 1966: Movement and predictability of radar echoes. *Tech. Memo ERTM-NSSL-28*, National Severe Storms Laboratory, 30 pp.
- Wilson, J. W., and D. L. Meigenhardt, 1997: Thunderstorm initiation, organization and lifetime associated with Florida boundary layer convergence lines. *Mon. Wea. Rev.*, **125**, 1507-1525.
- Wilson, J.W., N. A. Crook, C. K. Mueller, J. Sun and M. Dixon, 1998: Nowcasting Thunderstorms: A Status Report. *Bull. Amer. Meteor. Soc.*, **79**, 2079-2099.
- Wolfson, M.M., C.K. Mueller, and M. Eilts, 1997: Convective Weather Forecasting for FAA Applications by the Convective Weather Product Development Team. *7<sup>th</sup> Conference on Aviation, Range and Aero. Meteor.*, Amer. Met. Society, Long Beach, CA, 238-243.
- Wolfson, M.M., G.E. Forman, R.G. Hallowell, and M.P. Moore, 1998: The Growth and Decay Tracker. Preprints *8<sup>th</sup> Conference on Aviation, Range, and Aerospace Meteorology*, Amer. Met. Society, Dallas Tx. Pp 58-62.
- Wolfson, M.M, B.E. Forman, K.T. Calden, W.J. Dupree, R.J. Johnson Jr., R.A. Boldi, C.A. Wilson, P.E. Bieringer, E.B. Mann and J.P. Morgan, "Tactical 0-2 Hour Convective Weather Forecasts for FAA" 11th Conference on Aviation, Range, and Aerospace Meteorology, Hyannis, MA, 2004